The Meso-NH Atmospheric Simulation System:

Scientific Documentation

Part IV: Chemistry and Aerosols

Acknowledgments

This volume contains contributions from P. Bechtold, S. Belair, Ph. Bougeault, J.M. Carrière, J. Cuxart, V. Ducrocq, C. Fischer, M. Georgelin, P. Héreil, J.-P. Lafore, C. Liousse, C. Mari, I. Mallet, P. J. Mascart, V. Masson, J.-P. Pinty, E. Richard, K. Suhre, J. Stein, P. Tulet, and J. Vilà-Guerau de Arellano. As editors, we would like to express our deep appreciation for the dedicated work of all contributors. The Meso-NH project is the achievement of a much larger team. Our thanks extend to all those who are not cited here, but have given their best to create this unique tool.

Philippe Bougeault and Patrick Mascart

Since the 2002 edition, in addition to the contributors cited above, thanks have to be extended to C. Augros, F. Auguste, D. Barbary, C. Barthe, S. Berthet, Y. Bouteloup, C. Bovalo, O. Caumont, J.-P. Chaboureau, M. Chong, F. Couvreux, T. Dauhut, G. Delautier, J. Escobar, O. Geoffroy, P.A. Joulin, O. Nuissier, C. Lac, P. Le Moigne, M. Leriche, Q. Libois, T. Lunet, T. Marić, G. Molinié, T. Nagel, J. Pergaud, D. Ricard, Q. Rodier, R. Schoetter, F. Solmon, O. Thouron, M. Tomasini, B. Tsenova, B. Vié and F. Visentin.

Jean-Pierre Chaboureau

Chapter 1

Basics for the chemistry and aerosols

Contents

1.1 Overview

The present document describes the scientific aspects of the Meso-NH-chemistry code (MNHC in the following), i.e. the basic equations and the algorithms used to solve them, the initialization of the chemical variables, the treatment of the boundary conditions, the chemical reaction system presently implemented and how to modify it, and finally the zero dimensional version of Meso-NH-chemistry: the time-dependant box model. The objective of MNHC is to serve as a research tool for comprehensive atmospheric chemistry modeling at the mesoscale, the cloud scale and the turbulence scale (LES-chemistry), rather than as an operative model to forecast air quality. To meet this goal, it was essential to keep the chemical reaction scheme flexible and the formulations of rate constants general. Priority has thus been given to flexible solutions rather than to optimal computational performance. This version treats gas phase chemistry, bulk cloud chemistry and aerosol dynamics and chemistry.
A brief overview of the current state of MNHC is given here:

- MNHC is consistent with the following features of Meso-NH:
  - 0-D, 1-D, 2-D, and 3-D versions are supported in one code;
  - Meso-NH scalar variables are used to host the chemical variables, which means that boundary conditions, advection and turbulent transport are treated in the same way as for the Meso-NH water variables (refer to the corresponding documentation of these parts for details), i.e. full profit is taken from the positive advections schemes as well as the different parameterizations of turbulent mixing;

  - the chemistry part is coded such as to be coherent with Meso-NH grid-nesting and parallelization algorithms;
  - as the chemical calculations are mostly local, vectorization has been introduced on a line-by-line basis; that is every instruction is done in vectorized mode for a large number of grid points, thus yielding optimal performance on vectorizing architectures;
  - the box model (0-D) version is entirely compatible with the Meso-NH procedures and uses the same code as the multi-dimensional version.

- At each time step of Meso-NH and for each physical grid point a set of stiff differential equations describing the chemical evolution of the chemical variables is solved. Also at each point and each time step, the reaction rates are calculated as a function of the meteorological variables temperature, pressure, humidity, etc.

- The following chemical solvers are presently available: SIS, LinSSA, Cranck-Nicholson, EXQSSA (QSSA with extrapolation), SVODE (Gear-type) and Rosenbrock family solvers (recommended with cloud chemistry). Stiff solvers from the NAG library can be easily added, but are not activated for portability reasons (NAG is not available on all platforms).

- Several reaction schemes are presently implemented. The scheme implemented by default (ReLACS-AQ, Crassier et al. 2000; Leriche et al. 2013, see Annex 1.5) treats 41 chemical species in gas phase for 131 photo-chemical reactions. For gas phase, this scheme is a reduced version of RACM (Stockwell et al. 1997) and represents the state of the art in 3-D atmospheric chemistry modeling. In addition, for resolved clouds and if aqueous chemistry is activated, the scheme includes 25 additional chemical species in liquid phases (cloud water and rainwater) for 30 photo-chemical reactions and 20 reactions of exchange between gas and aqueous phase. Thus, 91 prognostic chemical species are considered in the cloud chemistry scheme completed by 24 more in iced precipitating hydrometeors if ice phase chemistry is activated.

- The implemented reaction scheme may be easily replaced by a completely different one. Starting from a file defining the reaction mechanism using a simple syntax, the corresponding Fortran90 subroutines are automatically generated. New reactions may thus be added easily.

- The following points are treated in a basic way, but need further development in the future:

  - Initialization of horizontally homogeneous fields using 1-D vertical profiles for the different chemical species is available either at the preparation of the dynamical fields (PREP_IDEAL_CASE program), or when the model is (re)started. The initialization with more realistic heterogeneous fields for real cases studies is provided by the large scale chemical model MOCAGE developed at Météo-France. Initialization of stratospheric ozone using an empirical PV-O_3 relationship have been tested successfully in the past but is not part of the present version of Meso-NH.
  - Photolysis rates can be read from a look-up table file, or may be calculated on-line with a radiative transfer model. In the 1-D version, modeled clouds may also be taken into account in the radiative algorithm. For the 3-D version, a parameterization is used to correct the clear-sky photolysis rates for cloud cover. Future developments will include coupling with the radiation scheme from Meso-NH for the effects of clouds on radiation.

- Lateral boundary conditions are treated by Meso-NH. There are thus no problems running with "cyclic" or "wall" boundary conditions, whereas the use of "open" boundaries requires extra coding by the user, that is the specification of the "large scale" forcing fields for the chemical variables.
- Temporal integration by Meso-NH is done using the "leapfrog" scheme (integration from time step $t - dt$ to $t + dt$, using time t to calculate the temporal derivative), whereas most stiff solvers work by definition in "forward" mode (integrating from time t to $t + dt$, using time t to advance in time). Three different methods to couple the temporal advance of Meso-NH with chemistry are implemented, using either a "split" technique or "centered" or "lagged" tendencies. An optimal coupling with respect to computing time would be the use of "forward" scalar variables in Meso-NH, which has not been implemented so far. The gain of a factor of nearly two in computing time should be possible when using this technique.

1.2 Basic equations

The dynamical part of Meso-NH can already carry an arbitrary number of passive scalars, following the equation:

$$\frac{\partial}{\partial t}\left(\rho_{\rm dref} s_*^{(i)}\right) + \boldsymbol{\nabla}\cdot\left(\rho_{\rm dref} s_*^{(i)} \boldsymbol{U}\right) = \rho_{\rm dref} \mathcal{S}_*^{(i)} \,, \tag{1.1}$$

where $\mathcal{S}_*^{(i)}$ stands for the effect of a diabatic or chemical process of the i-th scalar (chemical) variable. The treatment of advection and turbulent diffusion of the chemical species is treated elsewhere in this document, in this chapter only the chemical source/sink terms $\mathcal{S}_*^{(i)}$ are calculated. Given a reaction mechanism with $N_{\rm reac}$ reactions for $N_{\rm eq}$ prognostic chemical species, each reaction α between n_α reactants R_i and leading to the formation of m_α products P_j will be given as:

$$R_1 + R_2 + ... + R_{n_\alpha} \xrightarrow{k_\alpha} P_1 + P_2 + ... + P_{m_\alpha} \,, \tag{1.2}$$

where k_α is the n_α-th order reaction rate for reaction α. This defines for each reaction a term

$$T_\alpha = k_\alpha \prod_{l=1}^{n_\alpha} [R_l] \,. \tag{1.3}$$

The source terms $\mathcal{S}_*^{(i)}$ is then given by the expression:

$$\mathcal{S}_*^{(i)} = \sum_{\alpha=1}^{N_{\rm reac}} \sigma_{i\alpha} T_\alpha \,, \tag{1.4}$$

with

$$\sigma_{i\alpha} = \begin{cases} +1 & \text{if species } i \text{ is a product in reaction } \alpha \\ -1 & \text{if species } i \text{ is a reactant in reaction } \alpha \\ 0 & \text{otherwise} \end{cases} \,. \tag{1.5}$$

Note that species like O_2, N_2 and H_2O are usually treated as being constant and are thus taken into account in the expression of the reaction rate. They do not appear as prognostic variables. Unfortunately, due to big differences in the timescales of the chemical reactions, the system:

$$\frac{\partial}{\partial t} s_*^{(i)}\big|_{\rm chem} = \mathcal{S}_*^{(i)} \tag{1.6}$$

usually turns out to be what is called a "stiff" differential system (the lifetime of the different chemical species may vary by up to ten orders of magnitude). It is impossible to solve such a system with explicit methods, like Runge-Kutta or Euler-explicit. The required time step would be so small and the number of steps to be taken hence so big that the accumulation of numerical noise would destroy the physical solution. Special solvers like Gear's or other implicit methods have to be used. Also a number of fast hybrid methods, adapted to the specific problem of chemistry have been developed. Since there is no universal solver for those problems, a number of different solvers have been implemented that may be chosen as a function of the problem treated.
In order to solve the coupled set of equations (dynamics + chemistry), two possibilities exist: (a) use of operator splitting between transport and chemistry, and (b) use of tendencies. Both methods have been implemented. The algorithm for the "split" option is as follows:

1. integrate all physical contributions in variable `XRSVS` and calculate from that an intermediate solution for time step $t + dt$;

2. integrate with the stiff solver from $t - dt$ to $t + dt$, using that intermediate variable as initial value;

3. overwrite the variable `XRSVS` with the result from the solver.

The algorithm using tendencies (which is similar to the treatment of slow microphysics) allows for two options: using scalar variables at t ("centered") or at $t - dt$ ("lagged") as input for the solver. The algorithm is as follows:

1. integrate with the stiff solver from $t - dt$ to $t + dt$, using the variable `XSVT` ("centered") or `XSVM` ("lagged") as initial value;

2. add the tendency between the initial and the final value given by the solver to the contents of variable `XRSVS`.

The temporal integration of chemistry could be speed up by a factor of two if the scalar variables would be integrated using a forward scheme, which would have to be applied only every two time steps of the model. In this case, chemistry would also be called only every two time steps.

1.3 Stiff solvers

A solution of the system

$$\frac{d}{dt} y_i(t) = f_i(y, t) \tag{1.7}$$

is seek, where y denotes the vector of chemical concentrations ($i = 1, .., N_{\rm eq}$) and f the first derivative of the chemical system at every grid point of the dynamical model. Most of the computing time consumed by the chemistry part of Meso-NH is used by the stiff solver. The following methods are presently implemented:

SIS (Semi-implicit-symmetric): Ramaroson et al. (1992)
The method is linearized versions of the semi-implicit Euler method, meaning that for each time-step it needs a single inversion of a matrix of the dimension of the number of prognostic chemical

species. The method SIS may be written as:

$$y_i^{n+1} = y_i^n + \Delta t \left(I - \frac{\Delta t}{2} J^n \right)^{-1}_{ij} f_j^n \,, \tag{1.8}$$

where J is the Jacobian matrix of the system and y are the chemical concentrations at time $n\Delta t$ and $(n+1)\Delta t$.

LinSSA (linearized steady state approximation): Suhre and Rosset (1994)
The method LinSSA is a hybrid of SIS and QSSA, given as:

$$y_i^{n+1} = y_i^n + \Delta t \left(P - \frac{\Delta t}{2} J^n \right)^{-1}_{ij} \frac{1}{2} (P + I)_{jk} f_k^n \,, \tag{1.9}$$

with the projector P onto the prognostic variables defined as

$$P_{ij} = \begin{cases} 0 & i \neq j \text{ or } i = j \notin \mathcal{I} \\ 1 & i = j \in \mathcal{I} \end{cases} \,. \tag{1.10}$$

$\mathcal{I}$ is the index-set of the prognostic (not steady-state) variables.

Cranck-Nicholson: Stoer and Bulirsch (1978)
This is a standard implicit one-step method:

$$y^{n+1} = y_i^n + \Delta t \left(\alpha * f_i^n + (1 - \alpha) f_i^{n+1} \right) \,. \tag{1.11}$$

For $\alpha = 1$ it reduces to Euler-explicit and for $\alpha = 0$ to Euler-implicit. For $\alpha = 0.5$ this method can be shown to be of highest possible order for a one-step method. Its disadvantage is that a non-linear implicit equation has to be solved at each time step. Tests with typical chemical systems have shown that on average 4 matrix inversions are necessary in order to complete this task. Thus, the method is about 4 times more expensive than SIS and LinSSA, but therefore more precise.

QSSA (Quasi-Steady-State approximation): Hesstvedt et al. (1978)
The differential equation for chemistry can be rewritten as

$$\frac{d}{dt} y_i(t) = f_i(y,t) = P_i(y,t) - L_i(y,t) y_i \,, \tag{1.12}$$

where P_i and L_i are the production (where species i appears in the right hand side of a reaction) and loss terms (where species i appears in the left hand side of a reaction), respectively. Depending on the "lifetime" of species i, defined as $\tau_i = 1/L_i$, its integration is either performed with a simple Euler-explicit scheme (long-lived species), or using an analytic solution of equation (1.12) assuming P_i and L_i constant during a time step (life time of the order of the time step), or assuming a steady-state between production and loss (short-lived species). This can be expressed as follows:

$$y_i^{(n+1)} = y_i^n + \Delta t (P_i^n - L_i^n y_i^n) \qquad \text{for } \tau_i > 100\Delta t; \tag{1.13}$$

$$y_i^{(n+1)} = P_i^n / L_i^n \qquad \text{for } \tau_i < \Delta t/10; \tag{1.14}$$

$$y_i^{(n+1)} = P_i^n / L_i^n + (y_i^n - P_i^n / L_i^n) \exp(-L_i^n \Delta t) \qquad \text{otherwise.} \tag{1.15}$$

Rosenbrock family solvers: Sandu and Sander (2006)
Rosenbrock solvers are based on multistage implicit methods with an adaptative sub timestep to achieve a high order accuracy. These methods are also called linearly implicit Runge-Kutta methods (Durran 2010). The Rosenbrock methods are conservative and well adapted to solve stiff systems in cloud chemistry with slow and fast reaction rates in the gas and aqueous phases (Djouad et al. 2002). The s-stage method is given by:

$$y_{n+1} = y_n + \sum_{i=1}^{s} b_i k_i \tag{1.16}$$

where for i=1,...,s:

$$k_i = hf\left(t_n + \alpha_i h, y_n + \sum_{j=1}^{i-1} \alpha_{ij} k_j\right) + hJ \sum_{j=1}^{i} \gamma_{ij} k_j + \gamma_i h^2 \frac{\partial f}{\partial t}(t_n, y_n) \tag{1.17}$$

with:

$$\alpha_i = \sum_{j=1}^{i-1} \alpha_{ij}, \gamma_i = \sum_{j=1}^{i} \gamma_{ij} \tag{1.18}$$

$J = \partial f / \partial y$ is the jacobian matrix of the chemical system f. The set of coefficients b_i, α_{ij} and γ_{ij} are deduced from the s order accuracy condition requirements. Each stage of the method needs to solve a system of linear equations with unknowns k_i by inverting the matrix $I - h\gamma J$. This is done with an efficient LU-decompostion method that exploits the sparsity of J (only the non-zero coefficients are stored). The implementation of the family of Rosenbrock algorithm with $s \in 2, 3, 4$ in Meso-NH, is vectorized such that several independent chemical systems (one per grid point) are solved simultaneously.

1.4 Changing or adding reaction schemes

The chemical reaction scheme of MNHC is not coded directly in Fortran90, but using a "chemical definition file", which contains all necessary information in order to create the Fortran90 subroutines that calculate essentially the first derivative, the Jacobian of the system, the subroutines that calculate the reaction and photolysis rates, and some other utility subroutines. Here we give a brief summary of how this is done.
Suppose you wish to implement the following reaction scheme, which is actually an extract of the present reaction scheme RACM:

$$\begin{array}{lll} K_{001} = J_1 & : NO_2 & \longrightarrow \quad O(^3P) + NO \\ K_{024} = M \cdot 6.00 \cdot 10^{-34} (T/300)^{-2/3} & : O(^3P) + O_2 & \longrightarrow \quad O_3 \\ K_{048} = 2.00 \cdot 10^{-12} \exp(-1400/T) & : O_3 + NO & \longrightarrow \quad NO_2 + O_2 \end{array}$$

Then you have to write the following lines in your "chemical definition file" (for details of the syntax and additional options refer to book 3):

```
/begin_reactions/
K001 = !ZRATES(:,001)                          :: NO2       --> O3P + NO
K024 = TPK%M*6.00E-34*(TPK%T/300)**(-2.3) :: O3P + O2 --> O3
K048 = 2.00E-12*exp(-(1400.0/TPK%T))       :: O3  + NO --> NO2 + O2
/end_reactions/
```

The first line is a photolysis reaction, where ZRATES contains the photolysis rates at a given time and grid point. TPK%M is the concentration of air molecules, and TPK%T is the temperature. With respect to the earlier version of Meso-NH, the syntax of the chemical definition file has become somewhat more complex: The use of Fortran 90 types (indicated by %) is required by the grid-nesting, and the use of Fortran 90 vectors (indicated by :) is needed for the vectorization.
The preprocessor then translates these lines into Fortran90 code. An extract of the first derivative would look like this:

```
!PPROD(O3) = +K024*<O3P>*<O2>+...
 PPROD(:,1) = +TPK(:)%K024*PCONC(:,13)*TPK(:)%O2+...
!PLOSS(O3) = +K048*<NO>+...
 PLOSS(:,1) = +TPK(:)%K048*PCONC(:,3)+...
```

An extract of the Jacobian is:

```
!O3/O3=-K002-K003-K025*<O3P>-K029*<OH>-K030*<HO2>-K048*<NO>-K049*<NO2>-K106*<ET
!E>-K107*<OLT>-K108*<OLI>-K109*<DIEN>-K110*<ISO>-K111*<API>-K112*<LIM>-K113*<MA
!CR>-K114*<DCB>-K115*<TPAN>-K120*<ADDT>-K123*<ADDX>-K126*<ADDC>
 PJAC(:,1,1)=-TPK(:)%K002-TPK(:)%K003-TPK(:)%K025*PCONC(:,13)-TPK(:)%K029*PCONC&
&(:,15)-TPK(:)%K030*PCONC(:,16)-TPK(:)%K048*PCONC(:,3)-TPK(:)%K049*PCONC(:,4)-T&
&PK(:)%K106*PCONC(:,22)-TPK(:)%K107*PCONC(:,23)-TPK(:)%K108*PCONC(:,24)-TPK(:)%&
&K109*PCONC(:,25)-TPK(:)%K110*PCONC(:,26)-TPK(:)%K111*PCONC(:,27)-TPK(:)%K112*P&
&CONC(:,28)-TPK(:)%K113*PCONC(:,38)-TPK(:)%K114*PCONC(:,37)-TPK(:)%K115*PCONC(:&
&,43)-TPK(:)%K120*PCONC(:,59)-TPK(:)%K123*PCONC(:,60)-TPK(:)%K126*PCONC(:,61)
!
!O3/NO=-K048*<O3>
 PJAC(:,1,3)=-TPK(:)%K048*PCONC(:,1)
```

The subroutine that sets up the reaction and photolysis rates would contain the following lines:

```
TPK%M          = 1E-3*TPM%XMETEOVAR(2) * 6.0221367E+23 / 28.9644
TPK%T          = TPM%XMETEOVAR(3)
...
TPK(:)%K024=TPK%M*6.00E-34*(TPK%T/300)**(-2.3)
TPK(:)%K048=2.00E-12*exp(-(1400.0/TPK%T))
```

where the variable TPM%XMETEOVAR contains the meteorological fields, density (element 2), temperature (element 3), etc. A change of the reaction scheme is thus relatively "easy" and requires no extra Fortran90 coding by the user.

1.5 0-D box model

A time-dependant box model, using the same chemical reaction scheme and the same solver than MNHC is also available. In this case, the calculations that are done at every grid-point of Meso-NH are only done once, and all meteorological parameters that are used by the chemical system a read from a special file and may evolve in time. Conceptually, such a simplified model without dynamics can be obtained by integration of equation (1.1) over a fixed volume V:

$$\frac{\partial}{\partial t}\left\langle \rho_{\mathrm{dref}} s_*^{(i)} \right\rangle = \oint \rho_{\mathrm{dref}} \boldsymbol{F} \cdot d\boldsymbol{A} + \left\langle \rho_{\mathrm{dref}} \mathcal{S}_*^{(i)} \right\rangle , \tag{1.19}$$

where $\langle X \rangle = \frac{1}{V} \int X \, dV$ denotes volume averaging of the variable X, $\boldsymbol{F}$ is the flux through the boundaries **into** the volume V and $d\boldsymbol{A}$ the **outward** pointing surface element vector. Three cases are of interest: (a) the volume V represents the whole boundary layer, in this case the fluxes are the horizontal advection, the surface emission and dry deposition, and the boundary-layer/free-troposphere exchange flux; (b) the volume V represents a cylindric column of the boundary layer which will be moved around by the wind field, here no horizontal advection terms will be accounted for; and (c) the volume V represents a small air parcel, in this case no fluxes will be taken into account, the particle will be considered as being inert. For cases (a) and (b) instant and complete mixing of the whole boundary layer is assumed. Cases (b) and (c) are examples for so called "Lagrangian box models", external parameters like temperature, pressure, humidity, chemical concentrations etc. will be varied during the simulation. These parameters can be extracted from Meso-NH. A possible application is to run the 3D Meso-NH-chemistry model using a restricted reaction mechanism, then to trace Lagrangian trajectories in the model, and finally force the box-model with these parameters, allowing for the use of a more complex chemical reaction mechanism and possibly to drive an aerosol model with that data. Note that all external parameters of the box model can be time-dependant.

Such a simplified version of MNHC using only chemistry can also be used in order to test new reaction schemes, parameters for the solvers and chemical initial conditions prior to their use in a multi-dimensional version of Meso-NH.

The Regional Lumped Atmospheric Chemical Scheme - AQ

$$
\begin{aligned}
K_{001} &: NO_2 && \longrightarrow && O(^3P) + NO \\
K_{002} &: O_3 && \longrightarrow && O(^1D) + O_2 \\
K_{003} &: O_3 && \longrightarrow && O(^3P) + O_2 \\
K_{004} &: HONO && \longrightarrow && OH + NO \\
K_{005} &: HNO_3 && \longrightarrow && OH + NO_2 \\
K_{006} &: HNO_4 && \longrightarrow && 0.65 * HO_2 + 0.65 * NO_2 + 0.35 * OH + 0.35 * NO_3 \\
K_{007} &: NO_3 && \longrightarrow && NO + O_2 \\
K_{008} &: NO_3 && \longrightarrow && NO_2 + O(^3P) \\
K_{009} &: H_2O_2 && \longrightarrow && OH + OH \\
K_{010} &: HCHO && \longrightarrow && H_2 + CO \\
K_{011} &: HCHO && \longrightarrow && HO_2 + HO_2 + CO \\
K_{012} &: ALD && \longrightarrow && MO_2 + HO_2 + CO \\
K_{013} &: OP_1 && \longrightarrow && HCHO + HO_2 + OH \\
K_{014} &: OP_2 && \longrightarrow && 0.96205 * ALD + 0.96205 * HO_2 + 0.03795 * MO_2 + OH \\
K_{015} &: KET && \longrightarrow && 1.00000 * CARBOP + 1.00000 * ALKAP \\
K_{016} &: CARBO && \longrightarrow && 0.06517 * HCHO + 0.69622 * CARBOP + 0.75830 * HO_2 + \\
& && && 0.91924 * CO + 0.20842 * H_2 \\
K_{017} &: ONIT && \longrightarrow && 0.20 * ALD + 0.80 * KET + HO_2 + NO_2 \\
K_{018} &: O(^3P) + O_2 && \longrightarrow && O_3 \\
K_{019} &: O(^3P) + O_3 && \longrightarrow && 2.0 * O_2 \\
K_{020} &: O(^1D) + N_2 && \longrightarrow && O(^3P) + N_2 \\
K_{021} &: O(^1D) + O_2 && \longrightarrow && O(^3P) + O_2 \\
K_{022} &: O(^1D) + H_2O && \longrightarrow && OH + OH \\
K_{023} &: O_3 + OH && \longrightarrow && HO_2 + O_2 \\
K_{024} &: O_3 + HO_2 && \longrightarrow && OH + 2.0 * O_2
\end{aligned}
$$

$K_{025}: OH + HO_2 \longrightarrow H_2O + O_2$
$K_{026}: H_2O_2 + OH \longrightarrow HO_2 + H_2O$
$K_{027}: HO_2 + HO_2 \longrightarrow H_2O_2 + O_2$
$K_{028}: HO_2 + HO_2 + H_2O \longrightarrow H_2O_2 + H_2O + O_2$
$K_{029}: O(^3P) + NO \longrightarrow NO_2$
$K_{030}: O(^3P) + NO_2 \longrightarrow NO + O_2$

$K_{031}: O(^3P) + NO_2 \longrightarrow NO_3$
$K_{032}: OH + NO \longrightarrow HONO$
$K_{033}: OH + NO_2 \longrightarrow HNO_3$
$K_{034}: OH + NO_3 \longrightarrow NO_2 + HO_2$
$K_{035}: HO_2 + NO \longrightarrow NO_2 + OH$
$K_{036}: HO_2 + NO_2 \longrightarrow HNO_4$

$K_{037}: HNO_4 \longrightarrow HO_2 + NO_2$
$K_{038}: HO_2 + NO_3 \longrightarrow 0.3 * HNO_3 + 0.7 * NO_2 + 0.7 * OH$
$K_{039}: OH + HONO \longrightarrow H_2O + NO_2$
$K_{040}: OH + HNO_3 \longrightarrow NO_3 + H_2O$
$K_{041}: OH + HNO_4 \longrightarrow NO_2 + H_2O + O_2$
$K_{042}: O_3 + NO \longrightarrow NO_2 + O_2$

$K_{043}: O_3 + NO_2 \longrightarrow NO_3 + O_2$
$K_{044}: NO + NO + O_2 \longrightarrow NO_2 + NO_2$
$K_{045}: NO_3 + NO \longrightarrow NO_2 + NO_2$
$K_{046}: NO_3 + NO_2 \longrightarrow NO + NO_2 + O_2$
$K_{047}: NO_3 + NO_2 \longrightarrow N_2O_5$
$K_{048}: N_2O_5 \longrightarrow NO_2 + NO_3$

$K_{049}: NO_3 + NO_3 \longrightarrow NO_2 + NO_2 + O_2$
$K_{050}: NH_3 + OH \longrightarrow$
$K_{051}: OH + H_2 \longrightarrow H_2O + HO_2$
$K_{052}: OH + SO_2 \longrightarrow SULF + HO_2$
$K_{053}: CO + OH \longrightarrow HO_2 + CO_2$
$K_{054}: BIO + O(^3P) \longrightarrow 0.91868 * ALKE + 0.05 * HCHO + 0.02 * OH + 0.01 * CO + 0.13255 * CARBO + 0.28 * HO_2 + 0.15 * XO_2$

$K_{055}: CARBO + O(^3P) \longrightarrow ALD$
$K_{056}: CH_4 + OH \longrightarrow MO_2 + H_2O$
$K_{057}: ETH + OH \longrightarrow ALKAP$
$K_{058}: ALKA + OH \longrightarrow 0.87811 * ALKAP + 0.12793 * HO_2 + 0.08173 * ALD + 0.03498 * KET + 0.00835 * CARBO + 0.00140 * HCHO + 0.00878 * ORA_1 + 0.00878 * CO + 0.00878 * OH + H_2O$
$K_{059}: ALKE + OH \longrightarrow 1.02529 * ALKEP + 0.00000 * BIOP$
$K_{060}: BIO + OH \longrightarrow 1.00000 * BIOP$

$K_{061}: ARO + OH \longrightarrow 0.93968 * ADD + 0.10318 * XO_2 + 0.10318 * HO_2 + 0.00276 * PHO$
$K_{062}: HCHO + OH \longrightarrow HO_2 + CO + H_2O$
$K_{063}: ALD + OH \longrightarrow 1.00000 * CARBOP + H_2O$
$K_{064}: KET + OH \longrightarrow 1.00000 * CARBOP + H_2O$
$K_{065}: CARBO + OH \longrightarrow 0.51419 * CARBOP + 0.16919 * CARBO + 1.01732 * CO + 0.51208 * HO_2 + 0.00000 * HCHO + 0.06253 * ALD + 0.00853 * KET + 0.10162 * XO_2 + 0.75196 * H_2O$
$K_{066}: ORA_1 + OH \longrightarrow HO_2 + CO_2 + H_2O$

$K_{067}: ORA_2 + OH \longrightarrow$

$K_{068}: OP_1 + OH \longrightarrow 0.65 * MO_2 + 0.35 * HCHO + 0.35 * OH$

$K_{069}: OP_2 + OH \longrightarrow 0.40341 * ALKAP + 0.05413 * CARBOP + 0.07335 * ALD + 0.37591 * KET + 0.09333 * XO_2 + 0.02915 * HO_2 + 0.02915 * HCHO + 0.44925 * OH$

$K_{070}: PAN + OH \longrightarrow 0.57839 * HCHO + 0.21863 * CARBO + 0.71893 * NO_3 + 0.28107 * PAN + 0.28107 * HO_2 + 0.29733 * H_2O + XO_2$

$K_{071}: ONIT + OH \longrightarrow 1.00000 * ALKAP + NO_2 + H_2O$

$K_{072}: HCHO + NO_3 \longrightarrow HO_2 + HNO_3 + CO$

$K_{073}: ALD + NO_3 \longrightarrow 1.00000 * CARBOP + HNO_3$

$K_{074}: CARBO + NO_3 \longrightarrow 0.91567 * HNO_3 + 0.38881 * CARBOP + 0.10530 * CARBO + 0.05265 * ALD + 0.00632 * KET + 0.10530 * NO_2 + 0.10530 * XO_2 + 0.63217 * HO_2 + 1.33723 * CO + 0.00000 * OLN$

$K_{075}: ARO + NO_3 \longrightarrow HNO_3 + PHO$

$K_{076}: ALKE + NO_3 \longrightarrow 0.00000 * CARBO + 0.93768 * OLN$

$K_{077}: BIO + NO_3 \longrightarrow 0.91741 * CARBO + 1.00000 * OLN$

$K_{078}: PAN + NO_3 \longrightarrow 0.60 * ONIT + 0.60 * NO_3 + 0.40000 * PAN + 0.40 * HCHO + 0.40 * NO_2 + XO_2$

$K_{079}: ALKE + O_3 \longrightarrow 0.48290 * HCHO + 0.51468 * ALD + 0.07377 * KET + 0.00000 * CARBO + 0.35120 * CO + 0.15343 * ORA_1 + 0.08143 * ORA_2 + 0.23451 * HO_2 + 0.39435 * OH + 0.05705 * CARBOP + 0.03196 * ETH + 0.00000 * ALKE + 0.04300 * CH_4 + 0.13966 * MO_2 + 0.09815 * ALKAP + 0.01833 * H_2O_2 + 0.00000 * XO_2 + 0.05409 * H_2 + 0.00000 * O(^3P)$

$K_{080}: BIO + O_3 \longrightarrow 0.90000 * HCHO + 0.00000 * ALD + 0.00000 * KET + 0.39754 * CARBO + 0.36000 * CO + 0.37388 * ALKE + 0.00000 * ALKAP + 0.17000 * CARBOP + 0.03000 * MO_2 + 0.15000 * ORA_1 + 0.00000 * ORA_2 + 0.28000 * OH + 0.30000 * HO_2 + 0.00100 * H_2O_2 + 0.05000 * H_2 + 0.13000 * XO_2 + 0.09000 * O(^3P)$

$K_{081}: CARBO + O_3 \longrightarrow 0.00000 * HCHO + 1.07583 * CARBO + 0.15692 * ALD + 0.10788 * ORA_1 + 0.20595 * ORA_2 + 0.27460 * CARBOP + 0.10149 * OP_2 + 0.64728 * CO + 0.28441 * HO_2 + 0.20595 * OH + 0.00000 * H_2$

$K_{082}: PAN + O_3 \longrightarrow 0.70 * HCHO + 0.30000 * PAN + 0.70 * NO_2 + 0.13 * CO + 0.04 * H_2 + 0.11 * ORA_1 + 0.08 * HO_2 + 0.036 * OH + 0.70000 * CARBOP$

$K_{083}: PHO + NO_2 \longrightarrow 0.10670 * ARO + ONIT$

$K_{084}: PHO + HO_2 \longrightarrow 1.06698 * ARO$

$K_{085}: ADD + NO_2 \longrightarrow ARO + HONO$

$K_{086}: ADD + O_2 \longrightarrow 0.98 * AROP + 0.02 * ARO + 0.02 * HO_2$

$K_{087}: ADD + O_3 \longrightarrow ARO + OH$

$K_{088}: CARBOP + NO_2 \longrightarrow 1.00000 * PAN$

$K_{089}: PAN \longrightarrow 1.00000 * CARBOP + NO_2$

$K_{090}: MO_2 + NO \longrightarrow HCHO + HO_2 + NO_2$

$K_{091}: ALKAP + NO \longrightarrow 0.33144*ALD+0.03002*HCHO+0.54531*KET+0.03407*CARBO + 0.74265 * HO_2 + 0.09016 * MO_2 + 0.08187 * ALKAP+0.13007*XO_2+0.08459*ONIT+0.91541*NO_2$

$K_{092}: ALKEP + NO \longrightarrow 1.39870*HCHO+0.42125*ALD+0.05220*KET+HO_2+NO_2$

$K_{093}: BIOP + NO \longrightarrow 0.45463 * CARBO + 0.60600 * HCHO + 0.00000 * ALD + 0.00000*KET+0.37815*ALKE+0.84700*HO_2+0.84700*NO_2 + 0.15300 * ONIT$

$K_{094}: AROP + NO \longrightarrow 0.95115*NO_2+0.95115*HO_2+2.06993*CARBO+0.04885*ONIT$

$K_{095}: CARBOP + NO \longrightarrow 0.78134 * MO_2 + 0.09532 * CARBOP + 0.05848 * HCHO + 0.07368 * ALD + 0.08670 * CARBO + 0.12334 * HO_2 + 0.02563 * XO_2 + NO_2$

$K_{096}: OLN + NO \longrightarrow 0.18401*ONIT+1.81599*NO_2+0.18401*HO_2+0.23419*HCHO + 1.01182 * ALD + 0.37862 * KET$

$K_{097}: MO_2 + HO_2 \longrightarrow OP_1$

$K_{098}: ALKAP + HO_2 \longrightarrow 1.00524 * OP_2$

$K_{099}: ALKEP + HO_2 \longrightarrow 1.00524 * OP_2$

$K_{0100}: BIOP + HO_2 \longrightarrow 1.00524 * OP_2$

$K_{0101}: AROP + HO_2 \longrightarrow 1.00524 * OP_2$

$K_{0102}: CARBOP + HO_2 \longrightarrow 0.80904 * OP_2 + 0.17307 * ORA_2 + 0.17307 * O_3$

$K_{103}: OLN + HO_2 \longrightarrow ONIT$

$K_{104}: MO_2 + MO_2 \longrightarrow 1.33 * HCHO + 0.66 * HO_2$

$K_{105}: ALKAP + MO_2 \longrightarrow 0.80556*HCHO+0.98383*HO_2+0.56070*ALD+0.09673*KET+0.01390*MO_2+0.07976*CARBO+0.13370*XO_2+0.00385 * ALKAP$

$K_{106}: ALKEP + MO_2 \longrightarrow 1.42894 * HCHO + 0.46413 * ALD + 0.03814 * KET + HO_2$

$K_{107}: BIOP + MO_2 \longrightarrow 0.56064 * CARBO + 0.48074 * ALKE + 1.00000 * HO_2 + 1.09000 * HCHO + 0.00000 * ALD + 0.00000 * KET$

$K_{108}: AROP + MO_2 \longrightarrow HCHO + 1.02767 * HO_2 + 1.99461 * CARBO$

$K_{109}: CARBOP + MO_2 \longrightarrow 0.95723*HCHO+0.82998*HO_2+0.56031*MO_2+0.13684*ORA_2+0.05954*CARBOP+0.15387*CARBO+0.08295*ALD + 0.02212 * XO_2$

$K_{110}: OLN + MO_2 \longrightarrow 0.88625 * HCHO + 0.67560 * HO_2 + 0.67560 * ONIT + 0.41524 * ALD + 0.09667 * KET + 0.32440 * NO_2$

$K_{111}: ALKAP + CARBOP \longrightarrow 0.71461 * ALD + 0.48079 * HO_2 + 0.51480 * MO_2 + 0.49810 * ORA_2 + 0.18819 * KET + 0.07600 * HCHO + 0.00828 * ALKAP + 0.11306 * XO_2 + 0.06954 * CARBO$

$K_{112}: ALKEP + CARBOP \longrightarrow 0.68192*HCHO+0.68374*ALD+0.50078*HO_2+0.50078*MO_2 + 0.49922 * ORA_2 + 0.06579 * KET$

$K_{113}: BIOP+CARBOP \longrightarrow 0.78591 * CARBO + 0.24463 * ALKE + 0.50600 * HO_2 + 0.49400 * ORA_2 + 0.34000 * HCHO + 0.50600 * MO_2 + 0.00000 * ALD + 0.00000 * KET$

$K_{114}: AROP+CARBOP \longrightarrow MO_2 + HO_2 + 1.99455 * CARBO$

$K_{115}: CARBOP + CARBOP \longrightarrow 1.66702 * MO_2 + 0.05821 * CARBOP + 0.03432 * HCHO + 0.10777 * CARBO + 0.06969 * ALD + 0.02190 * KET + 0.07566 * HO_2 + 0.01593 * XO_2 + 0.09955 * ORA_2$

$K_{116}: OLN + CARBOP \longrightarrow 0.66562 * ONIT + 0.51037 * MO_2 + 0.48963 * ORA_2 + 0.17599 * HO_2 + 0.13414 * HCHO + 0.42122 * ALD + 0.10822 * KET + 0.00000 * NO_2$

$K_{117}: OLN + OLN \longrightarrow 2.00 * ONIT + HO_2$

$K_{118}: OLN + OLN \longrightarrow 0.00000 * HCHO + 0.00000 * ALD + 0.00000 * KET + 0.00000 * HO_2 + 0.00000 * NO_2 + 0.00000 * ONIT$

$K_{119}: MO_2 + NO_3 \longrightarrow HCHO + HO_2 + NO_2$

$K_{120}: ALKAP + NO_3 \longrightarrow 0.33743 * ALD + 0.81290 * HO_2 + 0.03142 * HCHO + 0.62978 * KET + 0.03531 * CARBO + 0.09731 * MO_2 + 0.08994 * ALKAP + 0.16271 * XO_2 + NO_2$

$K_{121}: ALKEP + NO_3 \longrightarrow 1.40909 * HCHO + 0.43039 * ALD + 0.02051 * KET + HO_2 + NO_2$

$K_{122}: BIOP + NO_3 \longrightarrow 0.61160 * CARBO + 0.42729 * ALKE + 0.68600 * HCHO + 0.00000 * ALD + 0.00000 * KET + HO_2 + NO_2$

$K_{123}: AROP + NO_3 \longrightarrow 2.81904 * CARBO + HO_2 + NO_2$

$K_{124}: CARBOP + NO_3 \longrightarrow 0.91910 * MO_2 + 0.03175 * CARBOP + 0.03175 * HCHO + 0.03455 * CARBO + 0.02936 * ALD + 0.04915 * HO_2 + 0.01021 * XO_2 + NO_2$

$K_{125}: OLN + NO_3 \longrightarrow 0.25928 * ONIT + 1.74072 * NO_2 + 0.25928 * HO_2 + 0.20740 * HCHO + 0.91850 * ALD + 0.34740 * KET$

$K_{126}: XO_2 + HO_2 \longrightarrow 1.00524 * OP_2$

$K_{127}: XO_2 + MO_2 \longrightarrow HCHO + HO_2$

$K_{128}: XO_2 + CARBOP \longrightarrow MO_2$

$K_{129}: XO_2 + XO_2 \longrightarrow$

$K_{130}: XO_2 + NO \longrightarrow NO_2$

$K_{131}: XO_2 + NO_3 \longrightarrow NO_2$

$KTC_1: O_3 \longrightarrow WC\_O_3$

$KTC_2: H_2O_2 \longrightarrow WC\_H_2O_2$

$KTC_3: NO \longrightarrow WC\_NO$

$KTC_4: NO_2 \longrightarrow WC\_NO_2$

$KTC_5: NO_3 \longrightarrow WC\_NO_3$

$KTC_6: N_2O_5 \longrightarrow WC\_N_2O_5$

$KTC_7: HONO \longrightarrow WC\_HONO$

$KTC_8: HNO_3 \longrightarrow WC\_HNO_3$

$KTC_9: HNO_4 \longrightarrow WC\_HNO_4$

$KTC_{10}: NH_3 \longrightarrow WC\_NH_3$

$KTC_{11}: OH \longrightarrow WC\_OH$

$KTC_{12}: HO_2 \longrightarrow WC\_HO_2$

$KTC_{13}: CO_2 \longrightarrow WC\_CO_2$

$KTC_{14}: SO_2 \longrightarrow WC\_SO_2$

$KTC_{15}: SULF \longrightarrow WC\_SULF$

$KTC_{16}: HCHO \longrightarrow WC\_HCHO$

$KTC_{17}: ORA_1 \longrightarrow WC\_ORA_1$

$KTC_{18}: ORA_2 \longrightarrow WC\_ORA_2$

$KTC_{19}: MO_2 \longrightarrow WC\_MO_2$

$KTC_{20} : OP_1 \longrightarrow WC\_OP_1$
$KTC_{21} : WC\_O_3 \longrightarrow O_3$
$KTC_{22} : WC\_H_2O_2 \longrightarrow H_2O_2$
$KTC_{23} : WC\_NO \longrightarrow NO$
$KTC_{24} : WC\_NO_2 \longrightarrow NO_2$
$KTC_{25} : WC\_NO_3 \longrightarrow NO_3$

$KTC_{26} : WC\_N_2O_5 \longrightarrow N_2O_5$
$KTC_{27} : WC\_HONO \longrightarrow HONO$
$KTC_{28} : WC\_HNO_3 \longrightarrow HNO_3$
$KTC_{29} : WC\_HNO_4 \longrightarrow HNO_4$
$KTC_{30} : WC\_NH_3 \longrightarrow NH_3$
$KTC_{31} : WC\_OH \longrightarrow OH$

$KTC_{32} : WC\_HO_2 \longrightarrow HO_2$
$KTC_{33} : WC\_CO_2 \longrightarrow CO_2$
$KTC_{34} : WC\_SO_2 \longrightarrow SO_2$
$KTC_{35} : WC\_SULF \longrightarrow SULF$
$KTC_{36} : WC\_HCHO \longrightarrow HCHO$
$KTC_{37} : WC\_ORA_1 \longrightarrow ORA_1$

$KTC_{38} : WC\_ORA_2 \longrightarrow ORA_2$
$KTC_{39} : WC\_MO_2 \longrightarrow MO_2$
$KTC_{40} : WC\_OP_1 \longrightarrow OP_1$
$KTR_1 : O_3 \longrightarrow WR\_O_3$
$KTR_2 : H_2O_2 \longrightarrow WR\_H_2O_2$
$KTR_3 : NO \longrightarrow WR\_NO$

$KTR_4 : NO_2 \longrightarrow WR\_NO_2$
$KTR_5 : NO_3 \longrightarrow WR\_NO_3$
$KTR_6 : N_2O_5 \longrightarrow WR\_N_2O_5$
$KTR_7 : HONO \longrightarrow WR\_HONO$
$KTR_8 : HNO_3 \longrightarrow WR\_HNO_3$
$KTR_9 : HNO_4 \longrightarrow WR\_HNO_4$

$KTR_{10} : NH_3 \longrightarrow WR\_NH_3$
$KTR_{11} : OH \longrightarrow WR\_OH$
$KTR_{12} : HO_2 \longrightarrow WR\_HO_2$
$KTR_{13} : CO_2 \longrightarrow WR\_CO_2$
$KTR_{14} : SO_2 \longrightarrow WR\_SO_2$
$KTR_{15} : SULF \longrightarrow WR\_SULF$

$KTR_{16} : HCHO \longrightarrow WR\_HCHO$
$KTR_{17} : ORA_1 \longrightarrow WR\_ORA_1$
$KTR_{18} : ORA_2 \longrightarrow WR\_ORA_2$
$KTR_{19} : MO_2 \longrightarrow WR\_MO_2$
$KTR_{20} : OP_1 \longrightarrow WR\_OP_1$
$KTR_{21} : WR\_O_3 \longrightarrow O_3$

$KTR_{22} : WR\_H_2O_2 \longrightarrow H_2O_2$
$KTR_{23} : WR\_NO \longrightarrow NO$
$KTR_{24} : WR\_NO_2 \longrightarrow NO_2$
$KTR_{25} : WR\_NO_3 \longrightarrow NO_3$
$KTR_{26} : WR\_N_2O_5 \longrightarrow N_2O_5$
$KTR_{27} : WR\_HONO \longrightarrow HONO$

$$
\begin{aligned}
KTR_{28}&: WR\_HNO_3 && \longrightarrow && HNO_3\\
KTR_{29}&: WR\_HNO_4 && \longrightarrow && HNO_4\\
KTR_{30}&: WR\_NH_3 && \longrightarrow && NH_3\\
KTR_{31}&: WR\_OH && \longrightarrow && OH\\
KTR_{32}&: WR\_HO_2 && \longrightarrow && HO_2\\
KTR_{33}&: WR\_CO_2 && \longrightarrow && CO_2
\end{aligned}
$$

$$
\begin{aligned}
KTR_{34}&: WR\_SO_2 && \longrightarrow && SO_2\\
KTR_{35}&: WR\_SULF && \longrightarrow && SULF\\
KTR_{36}&: WR\_HCHO && \longrightarrow && HCHO\\
KTR_{37}&: WR\_ORA_1 && \longrightarrow && ORA_1\\
KTR_{38}&: WR\_ORA_2 && \longrightarrow && ORA_2\\
KTR_{39}&: WR\_MO_2 && \longrightarrow && MO_2
\end{aligned}
$$

$$
\begin{aligned}
KTR_{40}&: WR\_OP_1 && \longrightarrow && OP_1\\
KC_1&: WC\_H_2O_2 && \longrightarrow && WC\_OH + WC\_OH\\
KC_2&: WC\_OH + WC\_OH && \longrightarrow && WC\_H_2O_2\\
KC_3&: WC\_OH + WC\_HO_2 && \longrightarrow &&\\
KC_4&: WC\_H_2O_2 + WC\_OH && \longrightarrow && WC\_HO_2\\
KC_5&: WC\_HO_2 + WC\_HO_2 && \longrightarrow && WC\_H_2O_2
\end{aligned}
$$

$$
\begin{aligned}
KC_6&: WC\_O_3 + WC\_HO_2 && \longrightarrow && WC\_OH\\
KC_7&: WC\_OH + WC\_SO_2 && \longrightarrow && WC\_ASO_3\\
KC_8&: WC\_HONO + WC\_OH && \longrightarrow && WC\_NO_2\\
KC_9&: WC\_NO_2 + WC\_HO_2 && \longrightarrow && WC\_HNO_4\\
KC_{10}&: WC\_HNO_4 && \longrightarrow && WC\_HO_2 + WC\_NO_2\\
KC_{11}&: WC\_HNO_4 && \longrightarrow && WC\_HONO
\end{aligned}
$$

$$
\begin{aligned}
KC_{12}&: WC\_HNO_4 + WC\_SO_2 && \longrightarrow && WC\_SULF + WC\_HNO_3\\
KC_{13}&: WC\_HNO_3 && \longrightarrow && WC\_NO_2 + WC\_OH\\
KC_{14}&: WC\_N_2O_5 && \longrightarrow && WC\_HNO_3 + WC\_HNO_3\\
KC_{15}&: WC\_NO_3 + WC\_SULF && \longrightarrow && WC\_HNO_3 + WC\_ASO_4\\
KC_{16}&: WC\_NO_3 + WC\_SO_2 && \longrightarrow && WC\_HNO_3 + WC\_ASO_3\\
KC_{17}&: WC\_MO_2 + WC\_MO_2 && \longrightarrow && 2.00 * WC\_HCHO + 2.00 * WC\_HO_2
\end{aligned}
$$

$$
\begin{array}{lll}
KC_{18}: WC\_MO_2 + WC\_SO_2 & \longrightarrow & WC\_OP_1 + WC\_ASO_3 \\
KC_{19}: WC\_HCHO + WC\_OH & \longrightarrow & WC\_ORA_1 + WC\_HO_2 \\
KC_{20}: WC\_ORA_1 + WC\_OH & \longrightarrow & WC\_CO_2 + WC\_HO_2 \\
KC_{21}: WC\_SO_2 + WC\_HCHO & \longrightarrow & WC\_AHMS \\
KC_{22}: WC\_AHMS & \longrightarrow & WC\_SO_2 + WC\_HCHO \\
KC_{23}: WC\_AHMS + WC\_OH & \longrightarrow & WC\_HO_2 + WC\_ORA_1 + WC\_SO_2 \\
KC_{24}: WC\_ASO_3 + W\_O_2 & \longrightarrow & WC\_ASO_5 \\
KC_{25}: WC\_ASO_5 + WC\_HO_2 & \longrightarrow & WC\_AHSO_5 \\
KC_{26}: WC\_ASO_5 + WC\_ASO_5 & \longrightarrow & WC\_ASO_4 + WC\_ASO_4 \\
KC_{27}: WC\_AHSO_5 + WC\_SO_2 & \longrightarrow & 2.00 * WC\_SULF \\
KC_{28}: WC\_ASO_4 & \longrightarrow & WC\_SULF + WC\_OH \\
KC_{29}: WC\_SO_2 + WC\_O_3 & \longrightarrow & WC\_SULF \\
KC_{30}: WC\_SO_2 + WC\_H_2O_2 & \longrightarrow & WC\_SULF \\
KR_1: WR\_H_2O_2 & \longrightarrow & WR\_OH + WR\_OH \\
KR_2: WR\_OH + WR\_OH & \longrightarrow & WR\_H_2O_2 \\
KR_3: WR\_OH + WR\_HO_2 & \longrightarrow & \\
KR_4: WR\_H_2O_2 + WR\_OH & \longrightarrow & WR\_HO_2 \\
KR_5: WR\_HO_2 + WR\_HO_2 & \longrightarrow & WR\_H_2O_2 \\
KR_6: WR\_O_3 + WR\_HO_2 & \longrightarrow & WR\_OH \\
KR_7: WR\_OH + WR\_SO_2 & \longrightarrow & WR\_ASO_3 \\
KR_8: WR\_HONO + WR\_OH & \longrightarrow & WR\_NO_2 \\
KR_9: WR\_NO_2 + WR\_HO_2 & \longrightarrow & WR\_HNO_4 \\
KR_{10}: WR\_HNO_4 & \longrightarrow & WR\_HO_2 + WR\_NO_2 \\
KR_{11}: WR\_HNO_4 & \longrightarrow & WR\_HONO \\
KR_{12}: WR\_HNO_4 + WR\_SO_2 & \longrightarrow & WR\_SULF + WR\_HNO_3 \\
KR_{13}: WR\_HNO_3 & \longrightarrow & WR\_NO_2 + WR\_OH \\
KR_{14}: WR\_N_2O_5 & \longrightarrow & WR\_HNO_3 + WR\_HNO_3 \\
KR_{15}: WR\_NO_3 + WR\_SULF & \longrightarrow & WR\_HNO_3 + WR\_ASO_4 \\
KR_{16}: WR\_NO_3 + WR\_SO_2 & \longrightarrow & WR\_HNO_3 + WR\_ASO_3 \\
KR_{17}: WR\_MO_2 + WR\_MO_2 & \longrightarrow & 2.00 * WR\_HCHO + 2.00 * WR\_HO_2
\end{array}
$$

$$
\begin{array}{lll}
KR_{18}: WR\_MO_2 + WR\_SO_2 & \longrightarrow & WR\_OP_1 + WR\_ASO_3 \\
KR_{19}: WR\_HCHO + WR\_OH & \longrightarrow & WR\_ORA_1 + WR\_HO_2 \\
KR_{20}: WR\_ORA_1 + WR\_OH & \longrightarrow & WR\_CO_2 + WR\_HO_2 \\
KR_{21}: WR\_SO_2 + WR\_HCHO & \longrightarrow & WR\_AHMS \\
KR_{22}: WR\_AHMS & \longrightarrow & WR\_SO_2 + WR\_HCHO \\
KR_{23}: WR\_AHMS + WR\_OH & \longrightarrow & WR\_HO_2 + WR\_ORA_1 + WR\_SO_2 \\
KR_{24}: WR\_ASO_3 + W\_O_2 & \longrightarrow & WR\_ASO_5 \\
KR_{25}: WR\_ASO_5 + WR\_HO_2 & \longrightarrow & WR\_AHSO_5 \\
KR_{26}: WR\_ASO_5 + WR\_ASO_5 & \longrightarrow & WR\_ASO_4 + WR\_ASO_4 \\
KR_{27}: WR\_AHSO_5 + WR\_SO_2 & \longrightarrow & 2.00 * WR\_SULF \\
KR_{28}: WR\_ASO_4 & \longrightarrow & WR\_SULF + WR\_OH \\
KR_{29}: WR\_SO_2 + WR\_O_3 & \longrightarrow & WR\_SULF \\
KR_{30}: WR\_SO_2 + WR\_H_2O_2 & \longrightarrow & WR\_SULF
\end{array}
$$

1.6 References

Crassier, V., K. Suhre, P. Tulet, and R. Rosset, 2000: Development of a reduced chemical scheme for use in mesoscale meteororological models. *Atm. Env.*, **34**, 2633–2644.

Djouad, R., B. Sportisse, and N. Audiffren, 2002: Numerical simulation of aqueous-phase atmospheric models: use of a non-autonomous Rosenbrock method. *Atm. Env.*, **36**, 873–879.

Durran, R. D., 2010: *Numerical methods for fluid dynamics with application to geophysics*. 2d ed., Springer, 516 pp.

Hesstvedt, E., O. Hov, and I. S. A. Isaksen, 1978: Quasi-steady stateapproximation in air pollution modelling: comparison of two numerical schemes for oxidant prediction. *Int. J. Chem. Kin.*, **10**, 4148–4156.

Leriche, M., J.-P. Pinty, C. Mari, and D. Gazen, 2013: A cloud chemistry module for the 3-D cloud-resolving mesoscale model Meso-NH with application to idealized cases. *Geosci. Model Dev.*, **6**, 1275–1298.

Ramaroson, R. A., M. Pirre, and D. Cariolle, 1992: A box model for on-line computations of diurnal variations in a 1-D model: potential for application in multidimensional cases. *Ann. Geophys.*, **10**, 416–428.

Sandu, A. and R. Sander, 2006: Modeling chemical kinetic systems in Fortran90 and Matlab with KPP-2.1. *Atm. Chem. Phys.*, **6**, 187–195.

Stockwell, R., F. Kirchner, M. Kuhn, and S. Seefeld, 1997: A new mechanism for regional atmospheric chemistry modeling. *J. Geophys. Res.*, **102**, 25 847–25 879.

Stoer, J. and R. Bulirsch, 1978: *Einführung in die Numerische Mathematik II*. Springer Verlag.

Suhre, K. and R. Rosset, 1994: Modification of a linearized semi-implicit scheme for chemical reactions using a steady-state-approximation. *Ann. Geophys.*, **12**, 359–361.

Chapter 2

Atmospheric Chemistry

Contents

This chapter reviews the main processes for the gas phase chemistry.

2.1 Dry deposition of gaseous species

The removal of gases from the atmosphere by turbulent transfer and uptake at the surface is defined as dry deposition. This process enables some chemically reactive gases to be efficiently removed from the atmosphere. Dry deposition of gaseaous specied was introduced in Meso-NH by Tulet et al. (2003). Dry deposition is usually parametrized through a deposition velocity v_d, defined by $v_d = -\frac{F_c}{c(z)}$, where F_c is the flux of the considered compound (F_c is assumed constant over the considered range of heights) and $c(z)$ is the concentration at height z (molecules/cm^3). v_d depends on many variables such as wind speed, temperature, radiation, the considered species and the surface conditions. It is commonly described through a resistance analogy often called "Big-Leaf" Model (e.g. Wesely and Hicks 1977).

$$v_d(z) = \frac{1}{R_a + R_b + R_c}$$

where R_a is the aerodynamic resistance, which is a function of the turbulence in the boundary layer, R_b the quasi-laminar resistance partially controlled by molecular diffusion, and R_c the surface resistance, which combines all the transfer pathways playing a role in the uptake of trace gases by the surface.

Meso-NH surface for dry deposition

As shown in Fig. 2.1, earth surface is divided into four major parts. On those surfaces calculation of specific parameters are done (friction velocities, surface resistances, ...). The earth splitting is done as follows : town horizontal fraction (Masson 2000), inland water and sea surfaces (differents because of their surface

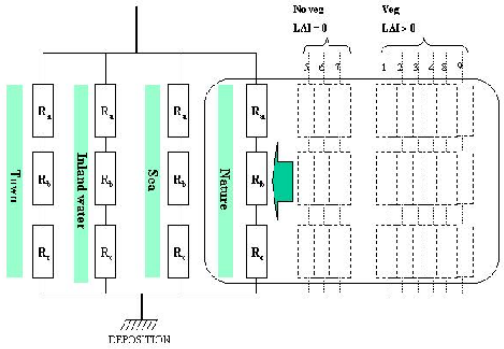

Figure 2.1: *Schematic resistances for dry deposition module in accordance with the surface state. Ra represents the aerodynamic resistance, Rb the quasi-laminar resistance and Rc the surface resistance.*

Meso-NH nature cover type	**Wesely correspondence class**
C3 cultures types(low)	(2) Agricultural land
C4 cultures types(hight)	(2) Agricultural land
forest and trees	(4) Deciduous and (5) coniferous forest
grassland	(3) Range land
no vegetation (smooth)	(8) Baren land, mostly desert
no vegetation (rocks)	(11) Rocky open areas with low-growing shrubs
permanent snow and ice	No correspondence
irrigated crops	(9) None forested wetland
irrigated parks gardens or peat bogs	(6) Mixed forest including weet land and (9) none forest wetland

Table 2.1: *Meso-NH vegetative cover type and Wesely connected class for dry deposition calculation*

temperature) and nature fractions. Nature surface is cut into 9 cover type, which can be reorganized by 'patches' (1 to 9). One 'patch' contains one or several cover types (user choice). These cover types are connected with the Wesely classes of vegetation for the surface resistance data parameters (see Table 2.1).

2.1.1 Resistances for dry deposition

Aerodynamic resistance R_a

R_a determines the rate of transport of gases between a given level in the atmosphere and the height of the effective surface sink. It is usually calculated as the bulk aerodynamic resistance to the transfer of momentum : $R_a(z_R) = \frac{1}{\mathbf{C_D V_A}}$, where $\mathbf{C_D}$ is the drag coefficient for momentum (see for example Wesely and Hicks 1977; Sheih et al. 1979; Walcek et al. 1986) and $\mathbf{V_A}$ the wind speed (in the following, the parameters which are already used or calculated in the MESO-NH subroutines will be noted in bold characters). The reference height z_R is taken as the lowest atmospheric level in the ISBA scheme.

An alternate way is to use the ISBA calculation of $\mathbf{R_a}$, $\mathbf{R_a(z_R)} = \frac{1}{\mathbf{C_H V_A}}$ which determines the transfer of

water vapor. $\mathbf{C_H}$ is then the drag coefficient depending upon the thermal stability of the atmosphere .
Heat drag coefficients are calculated in WATER_FLUX for inland water and sea, in URBAN for artificial land (town) and in ISBA for the other nature cover types or patch. So there is one $\mathbf{R_a}$ different for each different coefficient.
This formulation of $\mathbf{R_a}$ requires an additional term to the quasi-laminar resistance described below.

Quasi-laminar resistance R_b

The component R_b is associated with transfer through the quasi-laminar layer in contact with the surface. R_b quantifies the way in which pollutant or heat transfer differ from momentum transfer in the immediate vicinity of the surface (this is due to the effects of molecular diffusion and the difference of roughness lengths found for momentum and mass transfer). R_b depends on both turbulence characteristics and the molecular diffusion of the considered gas. Transport of a gas through the quasi-laminar layer by molecular diffusion depends on the thickness of the layer, the concentration gradient over the layer and on a diffusion constant, which in turn depends on the radius of the gas molecule and on the temperature. The complexity of vegetation generally limits the accuracy with which the magnitude of this mechanism can be estimated in the field. This resistance can be conveniently written as:

$$R_b = \frac{1}{ku^*} \log(\frac{z_0}{z_c})$$

k is the Von Karman constant and u^* the friction velocity. z_c is the roughness length for the pollutant under investigation (Baldocchi et al., 1987).
According to Hicks et al. (1987); Garrat and Hicks (1973) R_b can be approximated for vegetation and fibrous roughness elements by :

$$R_b = \frac{2}{\mathbf{ku}^*}(\frac{Sc}{Pr})^{2/3}$$

Sc and Pr are the Schmidt and Prandtl numbers respectively. $Pr = 0.72$ and $Sc = \frac{\nu}{D_i}$, with ν the kinematic viscosity of air (0.15 cm^2s^{-1}, 20° C, p = 1atm) and D_i the molecular diffusivity of gas i (see table 2.2 for some of these constants). For snow, ice, water and bare soil, R_b can be calculated by Ganzeveld and Lelieveld (1995):

$$R_b = \frac{1}{\mathbf{ku}^*}(\frac{Sc}{Pr})^{2/3}$$

This formulation is used for all Meso-NH grid fraction cover with no vegetation (Leaf Area Index = 0), that include artificial land, water and sea.
Definition of friction velocity in MNH is given by : $u^* = \sqrt[4]{< \mathbf{u'w'} >_{\mathbf{xx}}{}^2 + < \mathbf{v'w'} >_{\mathbf{xx}}{}^2}$. Where $< u'w' >_{xx}$ and $< v'w' >_{xx}$ represents surface fluxes of horizontal momentum in x and y directions (xx for sea, water, town and nature patch). Molecular diffusivity species/air can be obtain by the knowledge of H_2O/air diffusivity. The coefficient of diffusivity is given by the general formula as:
$D = vl/3 = 0.376kT\,/(N(MCste)^{0.5})$
with l mean free path, v mean molecular velocity, k Boltzmann constant, T temperature, N concentration, M molecular mass. So we use for computing molecular diffusivity:

$$D(gaz) = D(H_2O)\left(\frac{M(H_2O)}{M(gaz)}\right)^{0.5}$$

with

$$D(H_2O) = 2.22e-5 + 1.2510^{-7}(T+273) for 193K < T < 0K$$

$$D(H_2O) = 2.22e-5 + 1.4610^{-7}(T+273) for 273K < T < 323K$$

However, these formulations of R_b remain still controversial. Recent results from fields studies indicate that they are not in agreement with experimentally derived results, at least for the transfer of HNO_3 over wheat (Müller et al. 1993). At last, velocity dry deposition is not very sensitive of the choosen definition of R_b (Ganzeveld and Lelieveld 1995).

Surface Resistance R_c

The surface resistance is the most difficult of the three resistances to describe. R_c values can be obtained from theoretical considerations based for instance on solubility and equilibrium; calculations in combination with simulation of vegetation specific processes, such as accumulation, transfer process through stomata, mesophyll, cuticles, etc ... (Baldocchi et al. 1987; Wesely 1989). The values of R_c are based on measurements of V_d. By determining R_a and R_b from the meteorological measurements, R_c is calculated as the residual resistance. The calculated R_c are then related to surface conditions, time of day, etc ... in order to obtain parametrizations of R_c.

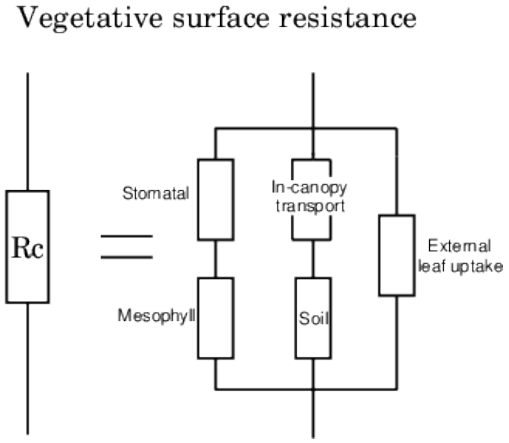

Figure 2.2: *Surface resistance schematic for vegetation.*

R_c is a function of the canopy stomatal resistance R_{stom} and mesophyll resistance R_m, the canopy cuticle or external leaf resistance R_{ext}, the soil resistance R_{soil} and in-canopy resistance R_{inc}, and the resistance to surface waters or moorland pools, R_{wat}, R_{sea} (Erisman 1994) In turn, these resistances are affected by leaf area index, stomatal physiology, soil and external leaf surface, pH presence and chemistry of liquid drops and films. In summary, R_c should be calculated as Erisman (1994):

- Vegetative surfaces : $R_c = \left(\frac{1}{R_{stom}+R_m} + \frac{1}{R_{inc}+R_{soil}} + \frac{1}{R_{ext}} \right)^{-1}$
- Water surfaces : $R_c = R_{wat}$
- Sea surfaces : $R_c = R_{sea}$
- Bare soil (no vegetation) : $R_c = R_{no}$
- Rock surfaces : $R_c = R_{rock}$
- Snow/ice cover : $R_c = R_{snow}$
- Artificial land : $R_c = R_{town}$

Species	Reactivity factor	Henry's law (M/atm)
Sulfur dioxide	0	$1.6(1 + 2.1\ 10^{-2}/H+)$
Nitric oxide	0	$1.9\ 10^{-3}$
Nitrogen dioxide	0.1	10^{-2}
Nitric acid	0	$5.8\ 10^{6}/H+$
Ozone	1.	$1.5\ 10^{-2}$
Hydrogen peroxide	0	$1.8\ 10^{5}$
Formaldehyde	0	$3.26\ 10^{-4}$
Aldehydes	0	76
Organic acids	0	$1.45\ 10^{-4}$
Organic peroxide	0.25	665
Peroxyacetic acid	0.5	1635
Peroxyacetyl nitrate	0.1	3.6
Other alkanes	0	$1.\ 10^{-3}$
Ethane	0	$1.9\ 10^{-3}$
Ethene	0	$4.9\ 10^{-3}$
Propene	0	$4.7\ 10^{-3}$
Butene and other olefins	0	$1.3\ 10^{-3}$
Toluene	0	0.15
Xylene	0	0.1

Table 2.2: *Reactivity factor and Henry's law constants for different chemical species*

Stomatal and mesophyll resistance R_{stom} and R_m

The stomatal resistance for water vapor is calculated in the ISBA subroutines as

$$\mathbf{R_{stom}} = \frac{\mathbf{R_{smin}}}{\mathbf{F_1 F_2 F_3 F_4\, LAI}},$$

where $\mathbf{LAI}$ is the leaf area index computed by patch, and F_1, F_2, F_3, F_4 are limiting factors depending on radiation, wetness of soil and temperature. In order to describe the stomatal resistance for another gas, the ISBA $\mathbf{R_{stom}}$ for water vapor should be corrected as followed :

$$R_{stom,x} = \mathbf{R_{stom}} \times \frac{D_{H_2O}}{D_x},$$

D_{H_2O} and D_x are the diffusion coefficients of H_2O and x respectively (Wesely 1989).

There is not much knowledge on the mesophyll resistance for different gases and the conditions which determine its value. For some gases, such as SO_2 O_3 and NH_3, R_m is experimentally found near zero values (Erisman 1994). This is in agreement with the parametrization suggested by Wesely (1989) for the calculation of the mesophyll resistance:

$$R_{mx} = (\frac{H^*}{3000} + 100 f_0)^{-1}$$

In this expression, H^* is the Henry's law constant for the considered gas, f_0 a reactivity factor which determines the rate of reduction of the substance. Two parallel pathways are thus assumed, one for highly reactive gases, the other one for soluble substances. Table 2.2 lists H^* and f_0 for some species (Baer and Nester 1992).

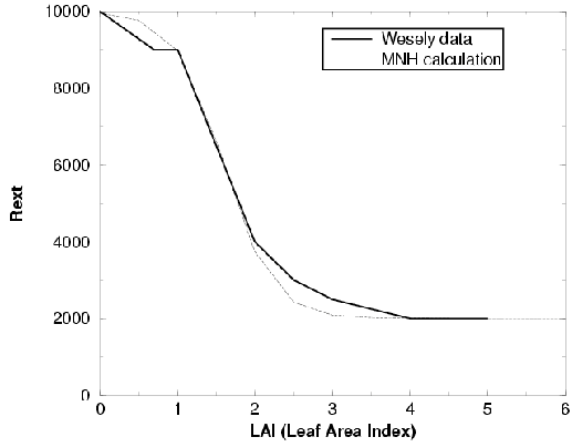

Figure 2.3: $\mathbf{R_{ext}}$ *fonction of* $\mathbf{LAI}$ *(from Wesely table)*

External leaf uptake R_{ext}

The external leaf uptake can act as an effective sink, especially for soluble gases at wet surfaces. The resistance of the outer surfaces in the upper canopy (leaf cuticular resistance in healthy vegetation) is computed by Wesely (1989), for a dry surface to any gas (x), as:

$$R_{ext.x.dry} = R_{ext}(10^{-5}H^* + f_0)^{-1}$$

In this expression, R_{ext} is given by land category and season in table 2.3, the constants (H^*, f_0) can be found in table 2.2.
The following equation is supposed to give an analytic expression of $\mathbf{R_{ext}}$ in accordance with Wesely table 2.3, and including seasonal variations through the leaf area index $\mathbf{LAI}$:

$$R_{ext} = 6000 - 4000\tanh(1.6(\mathbf{LAI} - 1.6))$$

These results had been compared with Wesely table in accordance with Méso-NH (ISBA) data of LAI (see Fig. 2.1.1).
In case of dew or rain, and according to the same author and (Walmsley and Wesely 1996), the equation should be replaced by :

$$R_{ext.x.wet} = [1/(3R_{ext.x.dry}) + (10^{-7}H^* + f_0/R_{extOzone}]^{-1}$$

with

- Rain:
$$R_{extOzone} = (1/(3R_{ext}) + 1/1000)^{-1}$$

- Dew:
$$R_{extOzone} = (1/(3R_{ext}) + 1/3000)^{-1}$$

To apply the same comput for each species we approximate in case of wet soil these formulas by using $R_{extOzone}$ as 3000 s/m.
These formulas should be corrected when surface temperature decreases below -2°C by adding the value $1000\exp(-T-4)$, in order to take into acccount the lesser uptake by surfaces when cold.

1	2	3	4	5	6	7	8	9	10	11
Midsummer with lush vegetation										
9999	2000	2000	2000	2000	2000	9999	9999	2500	2000	4000
Autumn with unharvested cropland										
9999	9000	9000	9000	4000	8000	9999	9999	9000	9000	9000
Late autumn after frost, no snow										
9999	9999	9000	9000	4000	8000	9999	9999	9000	9000	9000
Winter										
9999	9999	9999	9999	6000	9000	9999	9999	9000	9000	9000
Spring										
9999	4000	4000	4000	2000	3000	9999	9999	4000	4000	8000

Table 2.3: *Input resistances for calculation of external leaf resistance (Wesely 1989) : (1) urban land, (2) agricultural land, (3) range land, (4) deciduous forest, (5) coniferous forest, (6) mixed forest including wetland, (7) water, (8) barren land, mostly desert, (9) nonforested wetland, (10) mixed agricultural and range land, (11) rocky-open areas with low-growing shrubs*

In-canopy transport R_{inc}

Deposition to soils under vegetation can be relatively important. Meyers and Baldocchi (1988) found that 20% - 30% of SO_2 was deposited in summer to the soil under a deciduous forest. This transport is due to large-scale intermittent eddies through the vegetation. The corresponding resistance has been parametrized by Erisman (1994) using data of van Pul and Jacobs (1994) as:

$$R_{inc} = \frac{b\,\mathbf{LAI}\,h}{\mathbf{u}^*}$$

b is an empirical constant estimated at 14 m^{-1}. $\mathbf{LAI} = \mathbf{LAI\_patch}$ is the leaf area index given by patches computed in the GROUND_PARAMn files and $\mathbf{h}$ is the vegetation height which can be calculated as four times the vegetation roughness length (formula of Kondo and Yamazawa (1986), assuming a dense vegetation canopy with similar height).

Soil resitances for surfaces with no vegetation and those under vegetation

Table 2.4 presents a review of soil resistances for SO_2 and O_3 for clay, sand, snow and it is completed with Table 2.5, Wesely value for all other vegetation types, town and rock.
For other gases, the resistance can be computed following Wesely (1989) :

$$R_{soilx} = (\frac{H^*}{10^5 R_{soilSO_2}} + \frac{f_0}{R_{soilO_3}})^{-1}$$

According to the same author, this formula should be corrected when surface temperature decreases below -2°C by adding the value :

$$R_{soilx} = R_{soilx} + 1000\exp(-T-4)$$

For no vegetation cover soil surface composition (sand, clay) is considered. If it is covered by snow, this formlation will be update by using Table 2.4.

$$R_{sandx} = (\frac{H^*}{10^5 R_{sandSO_2}} + \frac{f_0}{R_{sandO_3}})^{-1}$$

Type of soil	SO_2	O_3
snow	540 at T <-1^{o}C	2000
	70(2-T) at -1 < T < 1	
sand	1000	200
clay	1000	100

Table 2.4: *Soil resistance*

$$R_{clayx} = (\frac{H^*}{10^5 R_{claySO_2}} + \frac{f_0}{R_{clayO_3}})^{-1}$$
$$R_{snowx} = (\frac{H^*}{10^5 R_{snowSO_2}} + \frac{f_0}{R_{snowO_3}})^{-1}$$

In this context $R_{no.x}$ for bare ground (no veg.) without snow is the weighted average of R_{sandx} and R_{clayx} as:

$$R_{no.x} = (\frac{\alpha_{sand}}{R_{sandx}} + \frac{\alpha_{clay}}{R_{clayx}})^{-1}$$

with
α_{sand} : percentage of sand in the ground
α_{clay} : percentage of clay in the ground
For all the other type of soil, resistance is calculated with Table 2.5 as:

$$\begin{aligned}
R_{rockx} &= (\frac{H^*}{10^5 R_{rockSO_2}} + \frac{f_0}{R_{rockO_3}})^{-1} \\
R_{townx} &= (\frac{H^*}{10^5 R_{townSO_2}} + \frac{f_0}{R_{townO_3}})^{-1} \\
R_{c3x} &= (\frac{H^*}{10^5 R_{c3SO_2}} + \frac{f_0}{R_{c3O_3}})^{-1} \\
R_{c4x} &= (\frac{H^*}{10^5 R_{c4SO_2}} + \frac{f_0}{R_{c4O_3}})^{-1} \\
R_{treex} &= (\frac{H^*}{10^5 R_{treeSO_2}} + \frac{f_0}{R_{treeO_3}})^{-1} \\
R_{grassx} &= (\frac{H^*}{10^5 R_{grassSO_2}} + \frac{f_0}{R_{grassO_3}})^{-1} \\
R_{irrx} &= (\frac{H^*}{10^5 R_{irrSO_2}} + \frac{f_0}{R_{irrO_3}})^{-1} \\
R_{parkx} &= (\frac{H^*}{10^5 R_{parkSO_2}} + \frac{f_0}{R_{parkO_3}})^{-1}
\end{aligned}$$

Surfaces resistances for sea and water

For deposition over water surface bodies, the surface resistance can be calculated from the expression recommended by Sehmel (1980) that incorporates wind speed and and air/water partitioning coefficient, rather than from Wesely's tabulated values for water bodies. The surface resistance over water is:

$$R_{waterx} = \frac{2,54.10^{-4}}{H^* \mathbf{T_{water}} \mathbf{u_*}} = Rc_{waterx}$$
$$R_{seax} = \frac{2,54.10^{-4}}{H^* \mathbf{T_{sea}} \mathbf{u_*}} = Rc_{seax}$$

MNH cover type									
c3	c4	tree	grass	no	rock	snow/ice	irr	park	town
Soil resistance for SO_2									
150	150	500	350	1000	400	no data	0	100	400
Soil resistance for O_3									
150	150	200	200	400	200	no data	1000	700	300

Table 2.5: *Soil resistance for MNH-C decomposition from Wesely table (quasi constant during the year). Values for "snow/ice" and "no" (no veg.) are not used see Table 2.4.*

2.1.2 Dry deposition velocity formulation

Artificial land resistance

$$Rglobal^{town} = Ra^{town} + Rb^{town} + Rc^{town}$$

Sea and water resistance

$$Rglobal^{water} = Ra^{water} + Rb^{water} + Rc^{water}$$

$$Rglobal^{sea} = Ra^{sea} + Rb^{sea} + Rc^{sea}$$

Nature final resistance

$$Rglobal^{nature} = \sum_{i=1}^{nvegtype} \left(\frac{\alpha_i}{Ra^{j_{patch}} + Rb^{j_{patch}} + Rc^{i}} \right)^{-1}$$

with
$i \overset{f}{\longmapsto} f(i) = j_{patch}$ like $i \in [1, nvegtype]$, $f(i) = j_{patch} \in [1, npatch \leq nvegtype]$
and α_i fraction of cover type (9 types)

Dry deposition velocity

Final dry deposition formulation:

$$v_{drydeposition} = \frac{\alpha_{water}}{Rglobal^{water}} + \frac{\alpha_{sea}}{Rglobal^{sea}} + \frac{\alpha_{townmax}}{Rglobal^{town}} + \frac{\alpha_{nature}}{Rglobal^{nature}}$$

where

α_{water} : fraction of water
α_{sea} : fraction of sea
$\alpha_{townmax}$: fraction of town increased
α_{sea} : fraction of nature

Fraction of town has to be increased in order to take account of the non negligible dry deposition on vertical surfaces in artificial area. The increase is done as follows:
$\alpha_{townmax} = \alpha_{town}(1 + 2\frac{H}{L}\,\alpha_{bld})$ with:
α_{town} horizontal fraction of town

H building height
L building caracteristic width
α_{bld} fraction of buildings in artificial areas (only)

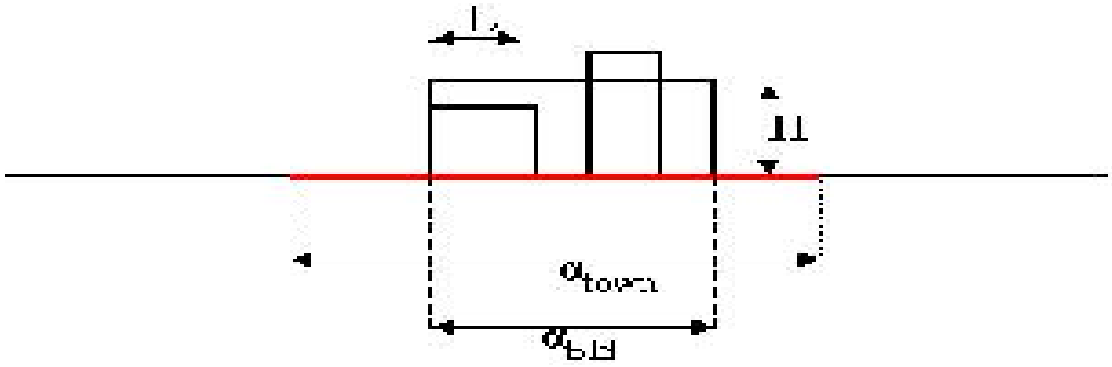

Figure 2.4: *town parameters in MNH (modd_gr_field) to increase fraction of town*

2.2 Photolysis rates

In 1-D version, photolysis rates are calculated on-line using the TUV algorithm (`http://www.acd.ucar.edu/TUV/`). In 3-D version, a look-up table is calculated for clear-sky photolysis rates using TUV model. The look-up table consists of photolysis rates at various altitudes, latitudes and hour angles. The look-up table is dependant upon the chemical mechanism. Within the model, photolysis rates for individual grid cells are interpolated from the look-up table. A parameterization is then used to correct the clear-sky photolysis rates for cloud cover.

2.2.1 Background

Many chemical reactions in the atmosphere are initiated by the photodissociation of numerous trace gases. These photodissociative reactions are responsible for most of the smog buildup detrimental to humans, animals, plant life and materials. In order to accurately model and predict the effects of air pollution, good photodissociation reaction rate (or photolysis rate) extimates must be made.
Photodissociation is the conversion of solar radiation into chemical energy to activate and dissociate chemical species. Species that photodissociate include many important trace constituents of the troposphere such as $O_3, NO_2, HONO, HNO_3, HNO_4, H_2O_2, HCHO, CH_3OOH$ (also see Appendix 1). The simulation accuracy of the entire chemical system is highly dependent upon the accuracy of photolysis rates, which are the primary sources of radicals in the troposphere. Photolysis rates (min^{-1}) sometimes called J-values, are computed for photodissociation reaction *(i)* by

$$J_i = \int_{\lambda_1}^{\lambda_2} F(\lambda)\sigma_i(\lambda)\Phi_i(\lambda)d\lambda$$

where, $F(\lambda)$ is the actinic flux (photons $\mathrm{cm}^{-2}\mathrm{min}^{-1}\mathrm{nm}^{-1}$), $\sigma_i(lambda)$ the absorption cross section for the molecule undergoing photodissociation ($\mathrm{cm}^2\mathrm{molecule}^{-1}$), $\Phi_i(\lambda)$ the quantum yield of the photolysis reaction (molecules photon^{-1}), and λ the wavelength (nm). Absorption cross section and quantum yields are functions of wavelength,and may also be functions of temperature and pressure; they are unique to species and reactions. Actinic flux is a radiometric quantity that measures the spectral radiance integrated

over all solid angles per unit area. The spherical receiving surface distinguishes the actinic flux from the more commonly measured irradiance, which is the radiance falling on a horizontal surface. Thus, the actinic flux can be called spherical spectral irradiance. The actinic flux changes with time of day, longitude, latitude, altitude, and season, and is governed by the astronomical and geometrical relationships between the sun and the earth. It is greatly affected by the earth's surface albedo as well as by various atmospheric scatterers and absorbers. Hence, correct model calculation of the temporal and spatial variation of the actinic flux is critical to obtaining accurate photolysis rates for regional and mesoscale modeling.
The current approach includes two stages of processing: (1) a table of clear sky photolysis rates is calculated for specified heights, latitudes and hours from local noon, and (2) photolysis rates are interpolated from the table based on grid cell location and the model time, and are corrected for cloud cover. This approach is computationally efficient and has been shown by Madronich (1987) to give clear-sky photolysis rates within the uncertainty of the surface-based measurements.

2.2.2 Cloud attenuation

The method used to correct for cloud cover is taken from Chang et al. (1987) and Madronich (1987). The correction of clear-sky values depends on whether the location is below, above, or within the cloud. The below cloud photolysis rate (J_{below}) is calculated as:

$$J_{below} = J_{clear}[1 + cfrac(1.6t_r \cos(\theta) - 1)]$$

where cfrac is the cloud coverage, θ is the zenith angle, and t_r is the cloud transmissivity. Below cloud photolysis rates will be lower than the clear-sky values due to reduced transmission of radiation through the cloud. The cloud transmissivity is calculated by:

$$t_r = \frac{5 - e^{-\tau_{cld}}}{4 + 3\tau_{cld}(1 - f)}$$

where f is the scattering phase function asymetry factor (assumed to be 0.86) and τ_{cld} id the cloud optical depth. The cloud optical depth equation is derived from Stephens (1978):

$$log(\tau_{cld}) = 0.2633 + 1.7095 \ln[\log(W)]$$

is only function of liquid path (W), where $\mathrm{W = L\Delta z(g/m^2)}$, L is the liquid water content ($\mathrm{g/m^3}$), and Δz is the cloud thickness. The above cloud top factor ($\mathrm{F_a}$) is calculated as:

$$J_{above} = J_{clear}[1 + cfrac(\alpha_i(1 - t_r)\cos(\theta)]$$

This equation allows for enhancement of photolysis rates above the cloud due to the reflected radiation from the cloud. It also includes a reaction dependent coefficient (α_i) which allows for further above cloud enhancements. Within the cloud, the cloud correction factor is a simple linear interpolation of the below cloud factor at cloud base to the above cloud factor at cloud top. Once computed, the below, above, and within cloud factor are used to scale the clear-sky photolysis rates to account for the presence of clouds. In the current implementation, all cloud types (including clouds composed of ice crystals) are treated the same using the above outlined procedure.

2.3 References

Baer, M. and K. Nester, 1992: Parameterization of trace gas dry deposition velocities for a regional mesoscale diffusion model. *Ann. Geophys.*, **10**, 912–923.

Chang, J., R. Brost, I. Isaksen, S. Madronich, P. Middleton, W. Stockwell, and C. Walcek, 1987: A three-dimensional eulerian acid deposition model: physical concepts and formulation. *J. Geophys. Res.*, **92**, 14 681–14 700.

Erisman, J., 1994: Evaluation of a surface resistance parameterization of sulphur dioxide. *Atmos. Environ.*, **16**, 2583–2594.

Ganzeveld, L. and L. Lelieveld, 1995: Dry deposition parameterization in a chemistry general circulation model and its influence on the distribution of reactive trace gases. *J. Geophys. Res.*, **100**, 20 999–21 012.

Garrat, J. and B. B. Hicks, 1973: Momentum, heat and water vapor transfer to and from natural and artificial surfaces. *Quart. J. Roy. Meteor. Soc.*, **99**, 680–687.

Hicks, B. B., D. D. Baldocchi, T. P. Meyers, R. P. Hosker, and D. R. Matt, 1987: A preliminary multiple resistance routine for deriving dry deposition velocities from measured quantities. *Water, Air and Soil Pollution*, **36**, 311–330.

Madronich, S., 1987: Photodissociation in the atmosphere: 1. Actinic flux and the effects of ground reflections and clouds. *J. Geophys. Res.*, **92**, 9740–9752.

Masson, V., 2000: A physically-based scheme for the urban energy budget in atmospheric models. *Bound.-Layer. Meteor.*, **94**, 357–397.

Meyers, T. P. and D. D. Baldocchi, 1988: A comparison of models for deriving dry deposition fluxes of O3 and SO2 to a forest canopy. *Tellus*, **40B**, 270–284.

Müller, H., F. X. Meixner, G. Kramm, D. Fowler, G. J. Dollard, and M. Possanzini, 1993: Determination of HNO_3 deposition by modified Bowen ratio and aerodynamic profile techniques. *Tellus*, **45B**, 346–367.

Sehmel, G. A., 1980: Particle and gas dry deposition: a review. *Atmos. Environ.*, **14**, 981–1011.

Sheih, C. M., M. L. Wesely, and B. B. Hicks, 1979: A guide for estimating dry deposition velocities of sulfur over the eastern united states and surrounding regions. *Argonne National Lab. Rep.*, **79-2**, 56.

Stephens, G. L., 1978: Radiation profiles in extended water clouds II Parameterization schemes. *J. Atmos. Sci.*, **35**, 2123–2132.

Tulet, P., V. Crassier, F. Solmon, D. Guedalia, and R. Rosset, 2003: Description of the Mesoscale Nonhydrostatic Chemistry model and application to a transboundary pollution episode between northern France and southern England. *J. Geophys. Res.*, **108(D1)**, 4021, doi.10.1029/2000JD000 301.

Walcek, C. J., R. A. Brost, J. S. Chang, and M. L. Wesely, 1986: so_2 sulfate and hno_3 deposition velocities computed using regional landuse and meterological data. *Atmos. Environ.*, **20**, 2101–2123.

Wesely, M. L. and B. B. Hicks, 1977: Some factors that affect the deposition rates of sulfur dioxide and similar gases to vegetation. *J. Air Poll. Control Assoc.*, **27**, 1110–1116.

Chapter 3

Clouds and chemistry

Contents

Clouds play an important role in atmospheric chemistry. Convective clouds transport pollutants vertically from the boundary layer to the upper troposphere. Clouds and associated precipitations scavenge pollutants from the air. Once inside the cloud or rain water, some compounds dissociate into ions and/or react with the one another through aqueous chemistry. Another important role for clouds is the removal of pollutants trapped in rain water and its deposition onto the ground. Clouds can also affect gas-phase chemistry by attenuating solar radiation below the cloud base, which has a significant impact on the photolysis reactions. The model currently incorporates parameterizations for sub-grid convective clouds (precipitating and non-precipitating) and for grid-scale resolved clouds.

3.1 Model description

The cloud scheme can be divided into two main components: the **sub-grid** cloud model and the **resolved** cloud model. For large horizontal grid resolutions, the grid size will be larger than the size of a typical convective cloud, requiring a parameterization for these sub-grid clouds. The sub-grid cloud scheme simulates convective precipitating and non-precipitation clouds (see Chapter:Convection Scheme). The second component of the cloud model considers clouds which occupy the entire grid cell and have been ”resolved”

by the model. The rate of change in pollutant concentrations (s_i) due to cloud processes is given by:

$$\frac{\partial C_i}{\partial t} = \frac{\partial C_i}{\partial t}_{subcld} + \frac{\partial C_i}{\partial t}_{rescld}$$

3.2 Subgrid convective cloud scheme

3.2.1 Wet scavenging

Scavenging by subgrid wet convective updrafts is applied within the convective mass transport algorithm (see Chapter:Convection Scheme) in order to prevent soluble tracers from being transported to the top of the convective updraft and then dispersed on the grid scale. The transport model provide wet convective air mass fluxes through each grid level in the updraft. As air is lifted a distance Δz from one level to the next, it loses a fraction $\mathrm{F_i}$ of soluble tracer i to scavenging. This fraction depends on (1) the rate constant k ($\mathrm{s^{-1}}$) for conversion of cloud condensate (including liquid and ice) to precipitation; (2) the fraction $f_{i,L}$ of tracer present in the liquid cloud condensate; (3) the fraction $f_{i,I}$ of tracer present in the ice cloud condensate; and (4) the retention efficiency R_i of tracer in the liquid cloud condensate as it is converted to precipitation ($R_i < 1$ accounts for volatilization during riming). Thus the rate constant k_i ($\mathrm{s^{-1}}$) for loss of tracer from the updraft is given by Mari et al. (2000):

$$k_i = (R_i f_{i,L} + f_{i,I})k$$

and the fraction F_i of tracer scavenged as the air is lifted by Δz is

$$F_i = 1 - \exp\left[-k_i \frac{\Delta z}{w}\right]$$

where w is the updraft velocity. The scavenged tracer is directly deposited to the surface, there can be no re-evaporation.

$\mathrm{HNO_3}$

$\mathrm{HNO_3}$ is 100% in the cloud condensate phase ($\mathrm{f_{i,L}} + \mathrm{f_{i,I}} = 1$) and we assume $R_i = 1$, therefore $k_i = k$ (Mari et al. 2000; Liu et al. 2001).

Gases other than $\mathrm{HNO_3}$

For gases other than $\mathrm{HNO_3}$, a significant fraction of tracer may be in the gas phase so that $k_i < k$. The phase partitioning of the tracer depends on the cloud liquid water content, L ($\mathrm{cm^3 water cm^{-3} air}$), and the cloud ice water content W ($\mathrm{cm^3 ice cm^{-3}}$ air).
Let $C_{i,G}, C_{i,L}, C_{i,I}, C_{i,T}$ represent the atmospheric mixing ratios of tracer in the gas, liquid, cloud condensate, ice cloud condensate, and all phases, respectively, so that

$$C_{i,T} = C_{i,G} + C_{i,L} + C_{i,I}$$

$$f_{i,L} = \frac{C_{i,L}}{C_{i,T}} = \frac{\frac{C_{i,L}}{C_{i,G}}}{1 + \frac{C_{i,L}}{C_{i,G}} + \frac{C_{i,I}}{C_{i,G}}}$$

$$f_{i,I} = \frac{C_{i,I}}{C_{i,T}} = \frac{\frac{C_{i,I}}{C_{i,G}}}{1 + \frac{C_{i,L}}{C_{i,G}} + \frac{C_{i,I}}{C_{i,G}}}$$

The ratio $C_{i,L}/C_{i,G}$ is obtained from Henry's law:

$$\frac{C_{i,L}}{C_{i,G}} = K_i^* LRT$$

where K_i^* (M atm^{-1}) is the effective Henry's law constant including contributions from dissociated species in fast equilibrium with the dissolved tracer, $R = 8.32 \times 10^{-2}$ atm M^{-1} K^{-1} is the ideal gas constant, and T is the local temperature in K. We calculate K_i^* from the van't Hoff equation:

$$K_i^* = K_{i298}^* \exp\left[-\frac{\Delta H_{i298}^0}{R}\left(\frac{1}{T} - \frac{1}{T_0}\right)\right]$$

where $T_0 = 298K$.
The retention efficiency R_i is unity for all gases in a warm cloud (T$\geq$268 K). Values of R_i in a mixed cloud ($248 <$ T < 268 K) are 0.02 for CH_3OOH and CH_2O and 0.05 for H_2O_2 (Mari et al. 2000).
The ratio $C_{i,I}/C_{i,G}$ for H_2O_2 is obtained by assuming scavenging by co-condensation:

$$\frac{C_{i,I}}{C_{i,G}} = \frac{W}{C_{H_2O}}\left(\frac{\alpha_{H_2O_2}}{\alpha_{H_2O}}\right)\left(\frac{M_{H_2O_2}}{M_{H_2O}}\right)^{\frac{1}{2}}$$

where C_{H_2O} is the water vapor mixing ratio (to be calculated from saturation over ice at the local temperature), $\alpha_{H_2O_2}/\alpha_{H_2O}$=0.6 is the ratio of sticking coefficients on the ice surface, and $M_{H_2O_2}/M_{H_2O}$=1.9 is the ratio of molecular weights.
For CH_3OOH and CH_2O scavenging by co-condensation is inefficient and we assume $C_{i,I}/C_{i,G}$=0.

3.2.2 Lightning produced NOx

The mass flux formalism applied to the convective transport of a chemical compound $\overline{C}$, writes :

$$\left.\frac{\partial \overline{C}}{\partial t}\right|_{convection} = -\frac{1}{\rho A}\frac{\partial (MC)}{\partial z} - \overline{w}\frac{\partial \overline{C}}{\partial z} \tag{3.1}$$

where A is the grid mesh area, ρ is the air density, M is the mass flux (in kg/s) and $\overline{w}$ is the environmental subsidence to compensate the upward mass flux. C is the mixing ratio of chemical compound in the convective cells. The mass flux term of Eq. (3.1) is further decomposed into:

$$\frac{\partial (MC)}{\partial z} = \frac{\partial (M^u C^u)}{\partial z} + \frac{\partial (M^d C^d)}{\partial z} \tag{3.2}$$

where the superscripts u and d refer to the "updrafts" and to the "downdrafts" components, respectively. The different mass flux divergences are expressed as:

$$\frac{\partial}{\partial z}(M^u C^u) = \epsilon^u \overline{C} - \delta^u C^u \tag{3.3}$$

$$\frac{\partial}{\partial z}(M^d C^d) = \epsilon^d \overline{C} - \delta^d C^d \tag{3.4}$$

where ϵ and δ are the parameterized entrainment and detrainment rates, respectively. Selecting C as the mixing ratio of nitrogen monoxide, $[NO]$, Eqs (3.3)-(3.4) are modified to include the internal LiNOx production rates (Mari et al. 2006):

$$\frac{\partial}{\partial z}(M^u [NO]^u) = \epsilon^u \overline{[NO]} - \delta^u [NO]^u + (\overline{\rho} A)\left.\frac{\partial [NO]^u}{\partial t}\right|_{LiNOx} \tag{3.5}$$

$$\frac{\partial}{\partial z}(M^d[NO]^d) = \epsilon^d\overline{[NO]} - \delta^d[NO]^d \tag{3.6}$$

The two terms on the right hand side of Eqs (3.5) and (3.6) represent the subgrid scale transport of NO. Transport of NO is assumed to take place instantaneously during each model timestep. The third term is the LiNOx term to be parameterized. It is worth noting that no a-priori vertical placement of LiNOx is necessary with this approach. Once produced inside the convective column, NO molecules are redistributed by upward and downward transport and detrained in the environment. The vertical placement of LiNOx is a direct consequence of the redistribution by mass fluxes inside the convective scheme.

The electrical activity in the thunderstorms is related to the vertical extension of the glaciated region where ice-ice particle rebounding collisions are efficient enough to explain the charging mechanisms (Reynolds et al. 1957; Takahashi 1978; Saunders 1992). A growing electrical field then results from the organization of dipolar, tripolar or even more complex charge structures at storm scale (Rust and MacGorman 2002; Rust and Marshall 1996; Stolzenburg et al. 2002; Barthe et al. 2005). The electrical field is broken down by a partial neutralization of the electrical charges. This is realized by a repetitive triggering of intra-cloud (IC) and cloud-to-ground (CG) flashes. The flashes lead to the formation of NO in the lightning channels after dissociation of air molecules at high temperature followed by a rapid cooling. According to the statistical regression formula of Price and Rind (1992), the total lightning frequency over land and ocean, f_f can be grossly estimated from mean cloud morphological parameters:

$$f_f = 3.44 \times 10^{-5} {H_{ct}}^{4.9} \tag{3.7}$$

over land and

$$f_f = 6.40 \times 10^{-4} {H_{ct}}^{1.73} \tag{3.8}$$

over ocean. H_{ct} is the cloud top height of the convective cells (in km).

Price and Rind (1993) proposed the following polynomial relationship between the thickness of the cold icy cloud (H_{fr} in km) and the IC/CG ratio, β:

$$\beta = 0.021H_{fr}^4 - 0.648H_{fr}^3 + 7.493H_{fr}^2 - 36.54H_{fr} + 63.09 \tag{3.9}$$

with $1 < \beta < 50$. A scaling factor $c_{pr} = 0.97241\ \exp(0.048203 \times \Delta lat \Delta lon)$ is introduced by Price and Rind (1994) to adapt f_f to different mesh sizes in interval of latitude (Δlat) and longitude (Δlon) given in degree.

The combination of Eqs (3.7)-(3.9), leads to the final expression of the LiNOx production rates to be inserted in Eq (3.5). It can be written in condensed form :

$$\left.\frac{\partial (NO)^u}{\partial t}\right|_{LiNOx} = \frac{\beta f_f}{1+\beta} \times P(IC) + \frac{f_f}{1+\beta} \times P(CG) \tag{3.10}$$

where the value of the mean production rate per CG and IC namely, $P(CG) = 6.7 \times 10^{26}$ of NO molecules, and $P(IC) = 6.7 \times 10^{25}$ of NO molecules, of Price et al. (1997) have been retained. It is worth noting that recent studies based on airborne observations and cloud scale modeling found that intracloud flashes are likely to be as effective in producing NO as cloud-to-ground flashes (DeCaria et al. 2000; Fehr et al. 2004; Ridley et al. 2005). It is also important to note that the estimates for the lightning NOx production based on Price and Rind (1992, 1994); Price et al. (1997) are on the high end of current estimates in the literature (Labrador et al. 2005).

The practical implementation of the LiNOx parameterization is based on critical vertical levels defined in the deep convection scheme. IC flashes are equally distributed between the cloud top and the freezing levels. The CGs are located between the -10°C level (or the level of free sink if below) and the ground. The NO production in flashes is assumed to be proportional to air density following Goldenbaum and Dickerson (1993). Recent studies have shown that unimodal or bimodal distributions would be more realistic than uniform distributions as discussed in MacGorman and Rust (1998); DeCaria et al. (2000, 2005).

3.3 Resolved Cloud Scheme

3.3.1 Cloud chemistry module

The cloud chemistry module allows solving both gaseous and aqueous phases chemistry as well as mass transfer reactions between gas and liquid phases and microphysical transfers of chemical species (Leriche et al. 2013). In nested mode, to avoid time computing, the cloud chemistry module can be available in the innest domain, the one at high resolution, while the coupling models (father models) treat the gas phase chemistry only. This possibility is obviously available in one–way nesting mode. The concentrations of chemical species i in gas phase and in aqueous phase (cloud water and rainwater) are solution of the set of differential equations:

$$\frac{\partial C_g^i}{\partial t}_{rescld} = \frac{\partial C_g^i}{\partial t}_{chem} + \frac{\partial C_g^i}{\partial t}_{emis} + \frac{\partial C_g^i}{\partial t}_{dep\_sec} + \frac{\partial C_g^i}{\partial t}_{mic} \tag{3.11}$$

$$\frac{\partial C_w^i}{\partial t}_{rescld} = \frac{\partial C_w^i}{\partial t}_{chem} + \frac{\partial C_w^i}{\partial t}_{mic} \tag{3.12}$$

The equation for gas phase is the same than without cloud except for the last term, which represents the release of soluble gases from the aqueous phase when evaporation occurs or when freezing or riming occurs. In equation for liquid phase, w stands for either cloud water or rainwater. The term mic represents the sources and sinks due to cloud microphysical processes. These terms depend on the cloud microphysics scheme used.

3.3.2 Chemical kinetic scheme

The evolution of the chemical concentrations (in mol per volume of air) in the gas phase and in liquid phases denoted by the term $chem$ above of a chemical species i are given by the generic set of differential equations:

$$\frac{\partial C_g^i}{\partial t}_{chem} = P_g^i - D_g^i C_g^i - k_{tw}^i \left(L_w C_g^i - \frac{C_w^i}{H_{eff}^i RT} \right) \tag{3.13}$$

$$\frac{\partial C_w^i}{\partial t}_{chem} = P_w^i - D_w^i C_w^i + k_{tw}^i \left(L_w C_g^i - \frac{C_w^i}{H_{eff}^i RT} \right) \tag{3.14}$$

Subcripts g and w are, respectively, for the gas phase and for liquid phases with w stands either for the cloud droplets or for the raindrops. Terms P and D are the production terms in mol per volume of air s^{-1} and the destruction terms in s^{-1}. L is the liquid water volume ratio (volume of the drops by volume of air) computed from the liquid water mixing ratio using air and water density. H_{eff} is the effective Henry's law constant in mol atm^{-1}. T is the temperature in K and R = 0.08206 atm mol^{-1} K^{-1} is the universal gas constant. The rate constant of transfer between the gas phase and the aqueous phase k_{tw} in s^{-1} is the inverse of the characteristic times for gaseous diffusion and for the interfacial mass transport according to Schwartz (1986):

$$k_{tw}^i = \left(\frac{a_w^2}{3D_g^i} + \frac{4a_w}{3\overline{v}^i \alpha^i} \right)^{-1} \tag{3.15}$$

the parameter a_w is the cloud droplet or raindrop radius in m, D_{gas} is the gaseous diffusion coefficient , $\overline{v}$ is the mean quadratic speed in m s^{-1} of the soluble species and α is the accommodation coefficient of the soluble species. The value of the drop radius for cloud droplets and raindrops comes from the microphysical scheme. In equations (3.13 and 3.14), the two first terms at the right hand side are the chemical production and destruction terms and the last term is the reversible uptake of soluble gases inside cloud droplets or

raindrops. The complete set of reactions of the cloud chemistry module is described in Leriche et al. (2013). This chemical mechanism called ReLACS-AQ has been developped based upon the gas phase mechanism ReLACS (Crassier et al. 2000) and includes 25 additional chemical species in liquid phases (cloud water and rainwater) for 30 photo-chemical reactions and 20 reactions of exchange between gas and aqueous phase. Thus, 91 prognostics chemical species are considered in the cloud chemistry scheme. The aqueous phase reactivity describes the reactivity of HO_x, of formadehyde and formic acid and of sulfur and nitrogen leading to the formation of sulfuric and nitric acid. All kinectic and thermodynamic data used are given in Leriche et al. (2013).

3.3.3 Microphysical transfer terms

Once dissolved or produced in the drops, the aqueous chemical species is redistributed between the cloud droplets and the raindrops by the cloud microphysical processes. Three processes are implied in the microphysical transfer of aqueous chemical species in cloud: autoconversion, accretion and sedimentation, which lead ultimately to the wet deposition of the soluble species by rain. These microphysical transfer terms are computed following:

$$\frac{\partial C_c^i}{\partial t}_{AUTO} = -\frac{\partial C_r^i}{\partial t}_{AUTO} = -C_c^i \frac{1}{r_c}\frac{\partial r_c}{\partial t}_{AUTO} \tag{3.16}$$

$$\frac{\partial C_c^i}{\partial t}_{ACCR} = -\frac{\partial C_r^i}{\partial t}_{ACCR} = -C_c^i \frac{1}{r_c}\frac{\partial r_c}{\partial t}_{ACCR} \tag{3.17}$$

$$\frac{\partial C_r^i}{\partial t}_{SEDI} = -C_r^i \frac{1}{r_r}\frac{\partial r_r}{\partial t}_{SEDI} = -C_r^i \frac{1}{r_r}\frac{\partial}{\partial z} F_{SEDI}\left(r_r\right) \tag{3.18}$$

r_c and r_r are the mass mixing ratios of the cloud droplets and of the raindrops, respectively. Subscripts AUTO, ACCR and SEDI are respectively for autoconversion process, accretion process and the sedimentation of the raindrops. F_{SEDI} is the sedimentation flux of the rain mixing ratio. The sedimentation flux and the tendencies of cloud droplets mixing ratio for autoconversion and accretion processes depend on the cloud microphysical scheme.

3.3.4 pH diagnostic equation

As the solubility of some important gaseous pollutants depends on the pH of the drops, and the chemical reactivity in the aqueous phase as well, it is crucial to predict the evolution of pH in cloud droplets and in raindrops. The pH is the solution of the electroneutrality equation which expresses the exact balance between the cations and the anions in an aqueous solution. By using a simplified form of the electroneutrality equation, the pH equation leads to a high order polynomial equation of the concentration of the protons $\mathrm{pH} = \log_{10}(\mathrm{H}^+)$. The physical root is found using the Laguerre method. In contrast with other technique (Barth et al. 2007), the pH is computed exactly and updated before each substep of the Rosenbrock algorithm to ensure numerical accuracy and stability of the aqueous phase reactions. Most of the coefficients of the pH polynomial equation are complex expressions containing reaction transfer rates. These expressions are automatically simplified using a formal calculus algorithm and not by hands to avoid errors.

3.3.5 Extension to the ice phase

In mixed phase clouds, additional processes for chemical species concentrations evolution appear including direct gas uptake by ice crystals, partitioning during freezing or riming of liquid hydrometeors and surface and bulk reactions in/on ice hydrometeors. Several studies have shown (Yin et al. 2002; Long et al. 2010) that the main process to be considered in the evolution of chemical species concentrations in mixed phase clouds is the retention of soluble gases when liquid hydrometeors freeze/rime. In particular, while the direct uptake inside growning ice crystals by vapor deposition is almost always negligeble, this process is not

implemented. The freezing and the riming of liquid drops transfer aqueous phase chemical species from liquid hydrometeors (cloud dropplets and raindrops) to precipitating iced hydrometeors i.e. snow, graupel and hail in Meso–NH. In order to limit the number of prognostic variables, the concentrations of chemical species in snow, graupel and hail have been treated globally as:

$$C^i_{ice} = C^i_{snow} + C^i_{grau} + C^i_{hail} \tag{3.19}$$

The additional microphysical transfer terms due to the retention of soluble gases during freezing/riming are computed following:

$$\frac{\partial C^i_g}{\partial t}_{FZ} = (1 - RET)\, C^i_w \frac{1}{r_w} \frac{\partial r_w}{\partial t}_{FZ} \tag{3.20}$$

$$\frac{\partial C^i_w}{\partial t}_{FZ} = -C^i_w \frac{1}{r_w} \frac{\partial r_w}{\partial t}_{FZ} \tag{3.21}$$

$$\frac{\partial C^i_{ice}}{\partial t}_{FZ} = RET C^i_w \frac{1}{r_w} \frac{\partial r_{ice}}{\partial t}_{FZ} = RET C^i_w \frac{1}{r_w} \left(\frac{\partial r_{snow}}{\partial t}_{FZ} + \frac{\partial r_{grau}}{\partial t}_{FZ} + \frac{\partial r_{hail}}{\partial t}_{FZ} \right) \tag{3.22}$$

$$\frac{\partial C^i_{ice}}{\partial t}_{SEDI} = -C^i_{ice} \frac{1}{r_{ice}} \frac{\partial r_{ice}}{\partial t}_{SEDI} = -C^i_{ice} \left(\frac{1}{r_{snow}} \frac{\partial r_{snow}}{\partial t}_{SEDI} + \frac{1}{r_{grau}} \frac{\partial r_{grau}}{\partial t}_{SEDI} + \frac{1}{r_{hail}} \frac{\partial r_{hail}}{\partial t}_{SEDI} \right) \tag{3.23}$$

FZ refers to freezing and riming processes. RET is the retention coefficient. A zero value for RET means that the soluble gas is completely released to the gas phase and is not retained in the ice phase at all. A value of 1 means that the soluble gas is completely retains in the ice phase. The last term $SEDI$ refers to the sedimentation of graupel, snow and hail, which contributes to wet deposition.

3.3.6 Lightning produced NOx at cloud scale

To be implemented

3.4 References

Barth, M. C., S.-W. Kim, W. C. Skamarock, A. L. Stuart, K. E. Pickering, and L. E. Ott, 2007: Simulations of the redistribution of formaldehyde, formic acid, and peroxides in the 10 July 1996 Stratospheric-Tropospheric Experiment: Radiation, Aerosols, and Ozone deep convection storm. *J. Geophys. Res.*, **112**, D13 310, doi:10.1029/2006JD008 046.

Barthe, C., G. Molinié, and J.-P. Pinty, 2005: Description and first results of an explicit electrical scheme in a 3D cloud resolving model. *Atmos. Res.*, **76**, 95–113.

DeCaria, A. J., K. E. Pickering, and G. L. S. et al., 2000: A cloud-scale model study of lightning-generated NO_x in an individual thunderstorm during STERAO-A. *J. Geophys. Res.*, **105**, 11 601–11 616.

DeCaria, A. J., K. E. Pickering, G. L. Stenchikov, and L. E. Ott, 2005: Lightning-generated NO_x and its impact on tropospheric ozone production: A three-dimensional modeling study of a Stratosphere-Troposphere Experiment: Radiation, Aerosols and Ozone (STERAO-A) thunderstorm. *J. Geophys. Res.*, **110**, D14 303.

Fehr, T., H. Holler, and H. Huntrieser, 2004: Model study on production and transport of lightning-produced NO_x in a EULINOX supercell storm. *J. Geophys. Res.*, **109**, D09 102.

Goldenbaum, G. C. and R. R. Dickerson, 1993: Nitric oxide production by lightning discharges. *J. Geophys. Res.*, **98**, 18 333–18 338.

Labrador, L. J., R. von Kuhlmann, and M. G. Lawrence, 2005: The effects of lightning-produced $\mathrm{NO_x}$ and its vertical distribution on atmospheric chemistry: Sensitivity simulations with MATCH-MPIC. *Atmos. Chem. Phys.*, **5**, 1815–1834.

Leriche, M., J.-P. Pinty, C. Mari, and D. Gazen, 2013: A cloud chemistry module for the 3-D cloud-resolving mesoscale model Meso-NH with application to idealized cases. *Geosci. Model Dev.*, in discussion.

Liu, H., D. J. Jacob, I. Bey, and R. M. Yantosca, 2001: Constraints from ^{210}pb and ^{7}be on wet deposition and transport in a global three-dimensional chemical tracer model driven by assimilated meteorological fields. *J. Geophys. Res.*, **106**, 12 109–12 128.

Long, Y., N. Chaumerliac, L. Deguillaume, M. Leriche, and F. Champeau, 2010: Effect of mixed phase cloud on the chemical budget of trace gases: a modeling approach. *Atmos. Res.*, **97**, 540–554.

MacGorman, D. R. and W. D. Rust, 1998: *The electrical nature of storms*. Oxford, 422 pp.

Mari, C., D. J. Jacob, and P. Bechtold, 2000: Transport and scavenging of soluble gases in a deep convective cloud. *J. Geophys. Res.*, **105**, 22 255–22 267.

Mari, C., et al., 2006: Regional lightning NOx sources during the TROCCINOX experiment. *Atmos. Chem. Phys.*, **6**, 5559–5572.

Price, C., J. Penner, and M. Prather, 1997: $\mathrm{NO_x}$ from lightning, Part I: Global distribution based on lightning physics. *J. Geophys. Res.*, **102**, 5929–5941.

Price, C. and D. Rind, 1992: A simple lightning parameterization for calculating global lightning distributions. *J. Geophys. Res.*, **97**, 9919–9933.

Price, C. and D. Rind, 1993: What determines the cloud-to-ground lightning fraction in thunderstorms? *Geophys. Res. Lett.*, **20**, 463–466.

Price, C. and D. Rind, 1994: Modeling global lightning distributions in a General Circulation Model. *Mon. Weather Rev.*, **122**, 1930–1939.

Reynolds, S. E., M. Brooks, and M. F. Gourley, 1957: Thunderstorm charge separation. *J. Meteor.*, **14**, 426–436.

Ridley, B. A., K. E. Pickering, and J. E. Dye, 2005: Comments on the parameterization of lightning-produced NO in global chemistry-transport models. *Atmos. Environ.*, **39**, 6184–6187.

Rust, W. and T. C. Marshall, 1996: On abandoning the thunderstorm tripole-charge paradigm. *J. Geophys. Res.*, **101**, 23 499–23 500.

Rust, W. D. and D. R. MacGorman, 2002: Possibly inverted-polarity electrical structures in thunderstorms during STEPS. *Geophys. Res. Lett.*, **29**, doi:10.1029/2001GL014 303.

Saunders, C. P. R., 1992: A review of thunderstorm electrification processes. *J. Appl. Meteorol.*, **32**, 642–655.

Schwartz, S. E., 1986: Mass-transport considerations pertinent to aqueous phase reactions of gases in liquid water clouds. *Chemistry of Multiphase Atmospheric Systems, NATO ASI Series, G6*, W. Jaeschke, Ed., Spinger-Verlag, The Netherlands, 415–471.

Stolzenburg, M., T. C. Marshall, W. D. Rust, and D. L. Bartels, 2002: Two simultaneous charge structures in thunderstorm convection. *J. Geophys. Res.*, **107**, doi:10.1029/2001JD000 904.

Takahashi, T., 1978: Riming electrification as a charge generation mechanism in thunderstorms. *J. Atmos. Sci.*, **35**, 1536–1548.

Yin, Y., K. S. Carslaw, and D. J. Parker, 2002: Redistribution of trace gases by convective clouds mixed-phase processes. *Atmos. Chem. Phys.*, **2**, 293–306.

Chapter 4

Aerosol Schemes

Contents

Aerosols are treated in two different ways in Meso-NH. First, aerosols are treated independently from the gas phase chemistry with a prescribed chemical composition. This is the case for dust or sea-salt aerosols. These aerosols however can interact with the radiative code and/or the cloud dynamics. Second, organic and inorganic aerosols (anthropogenic aerosols) can be fully coupled with the gas phase chemistry allowing subsequent interactions with gaseous source precursors.

4.1 Dust aerosols and sea salt

4.1.1 General theory

Dust is mobilized from dry desert surfaces when the wind friction speed reaches a threshold wind friction speed of approximately 0.2 m s^{-1}. Dust is an important aerosol with annual global emissions ranging from 1000 to 3000 Tg yr^{-1} and average global load around 10-30 Tg (Zender et al. 2004).
Dust aerosols both scatter and absorb solar radiation, and they absorb and re-emit terrestrial radiation. Since the dust is emitted to the atmosphere when there are large winds, dust emission often occur in the form of *dust storms* and optical depths near the source can be very large.
Sea salt aerosols are produced as film and jet droplets when bubbles, entrained in the water by breaking waves, disrupt the sea surface (Blanchard 1983), and at winds speeds exceeding about 9 m s^{-1}, by direct disruption of the wave tops (spume droplets) (Monahan et al. 1983). Sea salt play a major role acting as a marine CCN and modifying the marine clouds properties.

4.1.2 Sources and transport

A detailed description of the dust emissions processes is provided in a preceding chapter "Surface Processes Scheme".
Sea salt and dust are produced depending on the wind speed. The externalized surface of Meso-NH takes care of the mobilization, and sends moments of the size distribution to the atmospheric model. The size distributions of sea salt and dust are assumed to consist of three lognormal modes each, and these modes are described by their 0^{th}, 3^{rd} and 6^{th} moment. The moments can be transformed as diagnostic variables of the size distribution (σ (dispersion coefficient), r (median radius) and N (number concentration) following Tulet et al. (2005). The dust aerosols are parameterized following Grini et al. (2006). For emission processes, dust is mobilized using the Dust Entrainment And Deposition model (DEAD) (Zender et al. 2003) as a function of saltation and sandblasting as defined by Marticorena and Bergametti (1995). Sea salt emission is parameterized upon either the formulation of Vignati et al. (2001) (effective source function) or a lookup table defined by Schulz et al. (2004). Dust and sea salt are currently lost through sedimentation and rain out in convective clouds. The sedimentation takes into account the size of the aerosol where large particles have larger sedimentation velocity (see Sedimentation - Dry deposition in next section). The convective rainout is similar to gas chemistry and assumes that the aerosols are soluble in rain water with a solubility factor equal to 0.3. Explicit aqueous mass transfer of aerosol within clouds and rain droplets have been parameterized for dust, sea salt and anthropogenic aerosols (see section "Scavenging and aqueous mass transfer").

4.1.3 Radiation and optical properties

The dust influences the radiation scheme of Meso-NH. Optical properties in the short wave are calculated using the Mie code SHDOM (Evans 1998) *http://nit.colorado.edu/ evans/shdom.html* They are calculated off line, assuming a refractive index of:

- Ri[1]="(1.448,-0.00292)" for wavelengths comprises between 0.185 μm and 0.25 μm
- Ri[2]="(1.448,-0.00292)" for wavelengths comprises between 0.25 μm and 0.44 μm
- Ri[3]="(1.448,-0.00292)" for wavelengths comprises between 0.44 μm and 0.69 μm
- Ri[4]="(1.44023,-0.00116)" for wavelengths comprises between 0.69 μm and 1.19 μm
- Ri[5]="(1.41163,-0.00106)" for wavelengths comprises between 1.19 μm and 2.38 μm
- Ri[6]="(1.41163,-0.00106)" for wavelengths comprises between 2.38 μm and 4.0 μm

See Tulet et al. (2008) for more explanations.
The results of the Mie calculations are stored in a look up table as *asymetry factor* $[no\ unit]$, *single scattering albedo* $[no\ unit]$ and *extinction coefficient* $[m^2\ g^{-1}]$. These values are looked up as a function of wavelength, number median radius and dispersion coefficient of the aerosols.
The long wave code is not modified for special treatment of dust. There is a default *Longwave absorption coefficient* defined in *yoesw.f90* of the radiation code. The coefficient is used to calculated absorption of terrestrial radiation from optical depth at 550 nm. Although this treatment could be refined, the longwave effect of dust is supposed to be smaller than the shortwave effect (Myhre et al. 2003).

4.2 Organic and inorganic log-normal aerosols model (ORILAM)

The prognostic evolution of the aerosol size distribution is determined by a general dynamical equation (Friedlander 1977; Seinfeld and Pandis 1997) without analytical solution:

$$\frac{\partial n(r_p)}{\partial t} = f(n(r_p)) \tag{4.1}$$

where n is the function of aerosol size distribution (particles cm^{-3}) and r_p is the aerosol radius (μm). This equation can be integrated to obtain an equation system such as:

$$\frac{\partial M_k}{\partial t} = f(M_k) \tag{4.2}$$

where the k^{th} moment is given by $M_k = \int_0^\infty r_p^k n(r_p) dr_p$ (μm^k cm^{-3}). Using several assumptions (choice of the aerosol spectral distribution) the equation (4.2) can be closed giving $f(M_k)$ in terms of moments. Three modes have been implemented; the first one to represent the new particles formed (nuclei mode); the second one for bigger and evoluted particles (accumulation mode); the last one is devoted to dust particles and introduced as a passive mode (no interaction with the nuclei and accumulation mode). Each mode is represented by a log-normal distribution as:

$$n(\ln D) = \frac{N}{\sqrt{2\pi}\ln\sigma_g} \exp\left(-\frac{\ln^2(\frac{D}{D_g})}{2\ln^2(\sigma_g)}\right) \tag{4.3}$$

where N is the particle number concentration (in particles cm^{-3}), D is the particle diameter (μm) and D_g , σ_g are respectively the number median diameter and the geometric standard deviation of the modal distribution. The k^{th} moment of the mode i is defined as :

$$M_{k,i} = \int_0^\infty r^k n_i(r) dr \tag{4.4}$$

After integration (variable change as $x = \ln(r/D_g)/\ln(\sigma)$) we obtain:

$$M_{k,i} = N R_g^k \exp\left(\frac{k^2}{2}\ln^2(\sigma)\right) \tag{4.5}$$

A simple combination with equation (4.5) gives a relationship between M_k and the log-normal parameters σ_g, R_g and N:

$$N = M_0 \tag{4.6}$$

$$R_g = \left(\frac{M_3^4}{M_6 M_0^3}\right)^{1/6} \tag{4.7}$$

$$\sigma_g = \exp\left(\frac{1}{3}\sqrt{\ln\left(\frac{M_0 M_6}{M_3^2}\right)}\right) \tag{4.8}$$

For aerosol with many monomers, it is possible to modelize the aerosol size distribution by a continuous function n relative to mean radius r_p. The general dynamical equation is given by Friedlander (1977):

$$\frac{\partial n(r_p)}{\partial t} = (f_{convection} + f_{diffusion} + f_{coagulation} + f_{growth} + f_{sources/sink} + f_{external})(n(r_p)) \tag{4.9}$$

This equation can be integrated in terms of moments of the distribution as:

$$\frac{\partial M_k}{\partial t} = (f_{convection} + f_{diffusion} + f_{coagulation} + f_{growth} + f_{sources/sink} + f_{external})(M_k) \tag{4.10}$$

The aerosol dynamics are modeled as described by Whitby et al. (1991); Binkowski and Shankar (1995); Ackermann et al. (1998); Binkowski and Roselle (2003) with notable differences: (1) We chose to integrate 3 moments (0, 3 and 6th) as prognostic variables. This procedure permits us to keep all parameters of the modal distribution variable. (2) Different sets of parameterization of sulfate nucleation and inorganic

chemistry solvers are given. (3) The aerosol module is coupled on-line with meteorological fields and chemical species (organic condensation). (4) Sedimentation is integrated analytically for all moments. (5) Surface exchange is coupled to a mesoscale atmosphere/biosphere model.
One can note that the moments of order 0 and 3 are well known ; the integration of $M_k = \int_0^\infty r_p^k n(r_p) dr_p$ gives for $M_{0,i} = N_i$ where N_i is the total concentration of particles for mode i and $M_{3,i} = \frac{3}{4\Pi} V_i$ is a direct function of the total volume of mode i.

4.2.1 Coagulation

General description

Aerosol size distribution evolves by collision between particles, leading to coagulation process. Numerical cost of coagulation treatment is expensive but less expensive when a log-normal approach is used.
Several assumptions has been made to solve the binary coagulation: (1) A collision between two particles forms a new particle (2) The new particle is spherical (3) The new volume is equal to the sum of both initial particle volumes. Moments of the new particle formed after collision of particles of respective radius r_{p1} and r_{p2} is

$$r_{p12}^k = (r_{p1}^3 + r_{p2}^3)^{\frac{k}{3}} \tag{4.11}$$

It is necessary to consider coagulation as a transfer process of particles in the lognormal distribution: to update the moment evolution due to coagulation, we first consider the loss in moment due to extinction of both initial particles r_{p1} and r_{p2} (term $(r_{p1}^k + r_{p2}^k)$), and the supply of moment due to the creation of a new particle r_{p12} (term r_{p12}^k). The coagulation process can be integrated:

$$\begin{aligned}\frac{\partial M_k}{\partial t} &= \frac{1}{2}\int_0^\infty \int_0^\infty r_{p12}^k \beta(r_{p1}, r_{p2}) n(r_{p1}) n(r_{p2}) dr_{p1} dr_{p2} \\ &-\frac{1}{2}\int_0^\infty \int_0^\infty (r_{p1}^k + r_{p2}^k) \beta(r_{p1}, r_{p2}) n(r_{p1}) n(r_{p2}) dr_{p1} dr_{p2}\end{aligned} \tag{4.12}$$

with $\beta(r_{p1}, r_{p2})$ representing the coagulation rate between particles r_{p1} and r_{p2} in cm^3 s^{-1}.
For the particular case of $N = 2$, different modes i and j ($N > 2$ is an extrapolation of results below), we obtain from (4.12) and (4.11):

$$\begin{aligned}\frac{\partial M_k}{\partial t} &= \frac{1}{2}\int_0^\infty \int_0^\infty (r_{p1}^3 + r_{p2}^3)^{\frac{k}{3}} \beta(r_{p1}, r_{p2}) (n_i + n_j)(r_{p1}) (n_i + n_j)(r_{p2}) dr_{p1} dr_{p2} \\ &-\frac{1}{2}\int_0^\infty \int_0^\infty (r_{p1}^k + r_{p2}^k) \beta(r_{p1}, r_{p2}) (n_i + n_j)(r_{p1}) (n_i + n_j)(r_{p2}) dr_{p1} dr_{p2}\end{aligned} \tag{4.13}$$

It is easy to solve terms of equation (4.13) with the following convention: (1) When two particles collide in the same mode (intra-modal coagulation), the new one stays in this mode. (2) When two particles of different modes collide (inter-modal coagulation), the new one is in the mode with largest radius (here j). The second convention implies for the inter-modal coagulation that each particle of the lowest mode is transferred into the largest one. Nevertheless, the intra-modal coagulation of the lowest mode (i) is able to reach beyond the largest mode (j). As a consequence, we use an hybrid approach discussed by Ackermann et al. (1998). First, the model resolves the intersection diameter (d_{eq}) of both modes, with the equation:

$$\ln\left(\frac{N_i \ln \sigma_i}{N_j \ln \sigma_j}\right) = \frac{(\ln d_{eq} - \ln d_{pi})^2}{2 \ln^2 \sigma_{gi}} - \frac{(\ln d_{eq} - \ln d_{pj})^2}{2 \ln^2 \sigma_{gj}} \tag{4.14}$$

At the end of the time-step, particles of the lowest mode (Aitken mode) with diameter greater than d_{eq} are transferred into the largest one (Accumulation mode).

Coagulation rate

Coagulation is represented by an harmonic function which is an average between both coagulation limit regimes : 'free- molecular' and 'near continuum' (Whitby et al. 1991). Knudsen number defined by $Kn = \frac{\lambda}{r_p}$ permits to define the nature of the relationship between atmospheric gas and the particle. For $Kn < 0.1$, the particle is in a continuous fluid (continuum regime), whereas for $Kn > 10$ the particle moves as a gas molecule (free molecular regime).

- Free molecular regime $Kn > 10$

  In this regime, Friedlander (1977) gave the expression of coagulation rate as:

$$\beta^{fm}(r_{p1}, r_{p2}) = \left(\frac{6kT}{\rho_p}\right)^{\frac{1}{2}} \left(\frac{1}{r_{p1}^3} + \frac{1}{r_{p2}^3}\right)^{\frac{1}{2}} (r_{p1} + r_{p2})^2 \tag{4.15}$$

  To integrate this equation, we need to make the same assumption as in Lee et al. (1984):

$$\left(\frac{1}{r_{p1}^3} + \frac{1}{r_{p2}^3}\right)^{\frac{1}{2}} \approx \left(\frac{1}{r^{\frac{3}{2}}{}_{p1}} + \frac{1}{r^{\frac{3}{2}}{}_{p2}}\right) \tag{4.16}$$

  Now the equation (4.15) is written on the form:

$$\widetilde{\beta}^{fm}(r_{p1}, r_{p2}) = \left(\frac{6k_BT}{\rho_p}\right)^{\frac{1}{2}} \left(r_{p1}^{\frac{1}{2}} + 2\frac{r_{p2}}{r_{p1}^{\frac{1}{2}}} + \frac{r_{p2}^2}{r_{p1}^{\frac{3}{2}}} + \frac{r_{p1}^2}{r_{p2}^{\frac{3}{2}}} + 2\frac{r_{p1}}{r_{p2}^{\frac{1}{2}}} + r_{p2}^{\frac{1}{2}}\right) \tag{4.17}$$

  With this assumption, we can compute the variation of the moment due to coagulation process. But it is clear that this approximation is valid only in a short range of particle radius. To minimize the limitation of the approximation, a correction factor is defined as (for the mode i and k^{th} moment) :

$$b_{(6,i),intra} = \frac{\int_0^\infty \int_0^\infty r_{p1}^6 \beta^{fm} n_i(r_{p1}) n_i(r_{p2}) dr_{p1} dr_{p2}}{\int_0^\infty \int_0^\infty r_{p1}^6 \widetilde{\beta}^{fm} n_i(r_{p1}) n_i(r_{p2}) dr_{p1} dr_{p2}} \tag{4.18}$$

  These factors are tabulated in function of the log-normal parameters. Finally, we obtain:

$$\left(\frac{\partial M_{6,i}}{\partial t}\right)_{intra} \approx -b_{6,i,intra} \int_0^\infty \int_0^\infty r_{p1}^6 \widetilde{\beta}^{fm} n_i(r_{p1}) n_i(r_{p2}) dr_{p1} dr_{p2} \tag{4.19}$$

- Near-continuum regime $Kn < 1$

  For particles larger than their free mean path λ, Friedlander (1977) suggested the following expression for the coagulation rate:

$$\widetilde{\beta}^{nc}(r_{p1}, r_{p2}) = 4\Pi(D_{p1} + D_{p2})(r_{p1} + r_{p2}) \tag{4.20}$$

  where $D_p = (k_BTCc/6\Pi\mu r_p)$,
  the Cunningham coefficient $Cc = 1 + Kn(a + b\exp(-c/Kn))$, with a=1.126; b=0.42 and c= 0.87. Equation (4.20) cannot be integrated analytically. If we consider only the continuum/near-continuum regime, we can approximate Cc as:

$$Cc \approx 1 + A^{nc'} Kn \tag{4.21}$$

with $A^{nc'} = 1.392Kn^{0.0783}$. After substitution, equation (4.20) becomes:

$$\widetilde{\beta}^{nc}(r_{p1}, r_{p2}) = \frac{2k_B T}{3\mu}\left(2 + \lambda A_i^{nc'}\left(\frac{1}{r_{p1}} + \frac{r_{p2}}{r_{p1}^2}\right) + \lambda A_j^{nc'}\left(\frac{1}{r_{p2}} + \frac{r_{p1}}{r_{p2}^2}\right) + \frac{r_{p1}}{r_{p2}} + \frac{r_{p2}}{r_{p1}}\right) \quad (4.22)$$

As previously, correction factor can be considered. Nevertheless, the approximation used is precise enough in the continuum/near-continuum regime to be exempted.

- Generalization of Brownian Coagulation:
  Seinfeld and Pandis (1997) developed a general formulation for the coagulation rate $\beta(r_{p1}, r_{p2})$ using Fuchs (1964) formulation and a Cunningham coefficient due to Philips (1975). But the expression is too complicated to be integrated in a log-normal distribution approach. That is why Whitby et al. (1991) proposed an alternative solution to compute all coagulation coefficients averaging previously expression of free-molecule and near continuum regime as:

$$\frac{\partial M_k}{\partial t} \approx \frac{(\frac{\partial M_k}{\partial t})^{fm}(\frac{\partial M_k}{\partial t})^{nc}}{(\frac{\partial M_k}{\partial t})^{fm} + (\frac{\partial M_k}{\partial t})^{nc}} \quad (4.23)$$

4.2.2 Gas-particles conversion

Pre-existing particles grow by gaseous transfer upon their surface. A second way of gaseous-particles transfer is related to the formation of new particles by nucleation.
Just after the emission of a combustion particle, some of the gaseous species fix on the aerosol surface as an adsorption process. When these atmospheric molecules are either in sufficient number or on aerosol site with low curve radius, a phase change appears. At this stage, adsorption classical formalism on dry surface is not applicable. If the surface film is composed by an unique constituent in balance with the gas phase, when the atmospheric concentration of the constituent increases, molecules condense upon the aerosol surface to restore the thermodynamic balance.
The condensation process is discontinuous: the partial pressure needs to exceed a critical step to allow the phase change. In this case, the aerosol surface is crucial to transfer gaseous molecules into aerosol by condensation. The absorption process needs to have a pre-existing liquid film at the aerosol surface. The problem becomes different: as soon as a quantity of a species appears in gaseous phase, some molecules are transferred into particle phase by thermodynamical balance. In this model, we assume the aerosol is old enough to have a short liquid film at the surface. So, absorption has been retained as the dominant process of aerosol growth.
Gaseous species that interact with aerosol phase are from two different categories: mineral and organic species. Mineral species are fundamental to predict the condensation of water H_2O and thus the aerosol growth. Organic species include a large number of different species with particular specificity of solubility, saturation vapor pressure and hearthless. The organic aerosol fraction is able to modify the aerosol hygroscopic specificity. It is necessary to distinguish the organic matter issued from urban and rural areas. The first one is mainly primary (emitted) and hydrophobic whereas the second one is mainly secondary (condensed) and hydrophilic (Saxena et al. 1986).

Growth processing

Several parameters, such as temperature, relative humidity, total aerosol surface and the condensation matter rate determine which one is the principal growth factor of the aerosol. Whitby et al. (1991) gave the growth rate of the k^{th} moment relative to i mode as:

$$\frac{\partial M_{k,i}}{\partial t} = \frac{2k}{\Pi}\int_0^\infty r_p^{k-3}\Psi_p(r_p)n_i(r_p)dr_p \quad (4.24)$$

where Ψ_p is the condensation law on particles (μm^3 s^{-1}). Ψ_p can be separated in a Ψ_T and Ψ respectively independent and dependant on particle size.

$$\Psi_p = \Psi_T.\Psi \tag{4.25}$$

Equation (4.24) can be written as:

$$\frac{\partial M_{k,i}}{\partial t} = \frac{2k}{\Pi}\Psi_T I_{k,i} \tag{4.26}$$

with

$$I_{k,i} = \int_0^\infty r_p^{k-3}\Psi(r_p)n_i(r_p)dr_p \tag{4.27}$$

and

$$\Psi_T = \frac{m_w.(P_l - P_{surf,l})}{\rho_l RT} \tag{4.28}$$

where m_w is the molar mass of species l, P_l the partial pressure of species l, $P_{surf,l}$ the pressure of species l at the particle surface, ρ_l the volumic mass of l and T the ambient temperature of the system (the aerosol is supposed to be in thermal equilibrium with its environment). $\Psi(r_p)$ is the size contribution with two asymptotic forms:

- Free molecular regime;

$$\Psi^{fm} = \pi\alpha\bar{c}r_p^2 \tag{4.29}$$

  where α is the accommodation coefficient, $\bar{c}$ the kinetic velocity of vapor molecules ($\bar{c} = \sqrt{8RT/\pi m_w}$). Integration of equation (4.29) gives:

$$I_{k,i}^{fm} = \pi\alpha\bar{c}M_{k-1,i} \tag{4.30}$$

- Near continuum regime;

$$\Psi^{nc} = 4\pi D_v r_p \tag{4.31}$$

  where D_v the diffusivity of species l in the air. Integration of equation (4.31) gives:

$$I_{k,i}^{nc} = 4\pi D_v M_{k-2,i} \tag{4.32}$$

Finally, with the same average as for coagulation we can approximate the general form of $I_{k,i}$ as:

$$I_{k,i} = \frac{I_{k,i}^{fm} I_{k,i}^{nc}}{I_{k,i}^{fm} + I_{k,i}^{nc}} \tag{4.33}$$

Pratsini (1988) estimated that this kind of procedure to average growth process is a very good approximation in the transitional regime. In our model, we assume thermodynamical equilibrium ($P_l = P_{surf,l}$) in (4.28). We calculate $\delta\Psi_p$ as a diagnostic at the end of the timestep for use in (4.24).

Nucleation

To activate the nucleation process of aerosol, it is necessary to have the partial vapor pressure of gas species greater than associated saturated vapor pressure. Nevertheless there is few knowledge about nucleation of organic matter. In this model, only the sulfur nucleation is considered. We choose the Kulmala et al. (1998) parameterization for its consistence with the classical theory of binary homogeneous nucleation (Wilemski 1984) and for taking into account the hydratation effect. The nucleation rate is parameterized as:

$$\begin{aligned} J = \exp\Bigg(&25.1289N_{sulf} - 4890.8\frac{N_{sulf}}{T} - \frac{1743.3}{T} \\ &-2.2479\delta N_{sulf}RH + 7643.4\frac{x_{al}}{T} - 1.9712\frac{x_{al}}{RH}\Bigg) \end{aligned} \tag{4.34}$$

with $x_{al} = 1.2233 - \frac{0.0154RA}{RA+RH} + 0.0102\ln(N_{av}) - 0.0415\ln(N_{wv}) + 0.0016T$ the molar fraction of H_2SO_4 in the critical nucleus (stable);
N_{av} and N_{wv} respectively the concentration of sulfuric acid vapor and water vapor in cm^{-3};
T the atmospheric temperature (K), RA and RH absolute and relative humidity. $N_{sulf} = \ln\left(N_a/exp(-14.5125 + 0.1335T - 10.5462RH + 1958.4(RH/T))\right)$ is the logarithm ratio between N_a (ambient concentration of sulfur acid in cm^{-3}) and $N_{a,c}$ the concentration sulfur acid need to reach a nucleation rate of $J = 1$ cm^{-3} s^{-1}; and $\delta = 1 + \frac{T-273.15}{273.15}$. $N_{a,c}$ can be given by:

$$N_{a,c} = \exp(-14.5125 + 0.1335T - 10.5462RH + 1958.4(RH/T)) \tag{4.35}$$

Mineral thermodynamic balance

In this version, two sets of mineral thermodynamical equilibrium has been introduced for the prediction of the balance between aerosol and gas phases of the system NH_3- SO_4-HNO_3-H_2O. The first parameterization is ARES, a revised version of MARS (Saxena et al. 1986), developed by Binkowski and Shankar (1995). The second parameterization introduced is ISORROPIA from Nenes et al. (1998).

Heterogenous chemistry

The aerosol phase can modify the gaseous composition by heterogeneous and multiphase reactions (Ravishankara 1997). Following Jacob (2000), we introduced the minimal set of reactions which is presented here with their associated uptake coefficients λ to improve the ozone model:

$$HO_2 \rightarrow 0.5H_2O_2 \qquad \lambda = 0.2 \tag{4.36}$$

$$NO_3 \rightarrow HNO_3 \qquad \lambda = 10^{-3} \tag{4.37}$$

$$NO_2 \rightarrow 0.5HNO_3 + 0.5HONO \qquad \lambda = 10^{-4} \tag{4.38}$$

$$N_2O_5 \rightarrow 2HNO_3 \qquad \lambda \in [0.01, 1] \tag{4.39}$$

The first order rate constant for gas heterogeneous loss onto particles is given by:

$$ka = \sum_k \left(\frac{d_k}{2D_g} + \frac{4}{\nu\lambda}\right)^{-1} A_k \tag{4.40}$$

with d_k the particle diameter (m), D_g the reacting gas molecular diffusivity (m^2 s^{-1}), μ the mean molecular velocity (m s^{-1}), A_k the total surface area of mode k and λ the uptake coefficient of reactive species.

Organic condensation

In the troposphere, Volatil Organic Compounds (VOCs) are mainly oxidized by OH radical, NO_3 and O_3. Some of these products have a very low saturated vapor pressure to be absorbed and form SOA (secondary organic aerosol). To take into account correct condensation process we need to restore thermodynamical balance for all species. With this aim, some new chemical schemes, such as CACM (Griffin et al. 2002) distinguish VOCs products in accordance with their capability to condense on the aerosol phase. The default scheme (ReLACS) do not allow these secondary organic aerosol parent: in this case the use of ORILAM do not compute organic condensation. Otherwise, using CACM scheme (or it's reduced version ReLACS2), one can active two different set of organic thermodynamic balance which are MPMPO (Griffin et al. 2005) and the AER module of Pun et al. (2002). The SOA precursor lumped groups are partitioned to distinguish hydrophobic, hydrophilic structural characteristics Pun et al. (2002) together with sources (biogenic versus anthropogenic), volatility and potential dissociation (Griffin et al. 2005), chemical and structural characteristics defined by Pun et al. (2002) in previous applications of CACM. The predictions of lumped SOA

precursors can be coupled with thermodynamic equilibrium modules for aerosol prediction. SOA are group into ten different aerosol class. To active SOA, it is necessary to compile CACM.chf or ReLACS.chf using the preprocessor m9 (or m10).

4.2.3 Dry deposition and sedimentation

Dry deposition and sedimentation of aerosols are driven by the Brownian diffusivity:

$$D_p = \left(\frac{kT}{6\pi\nu\rho_{air}r_p}\right) C_c \tag{4.41}$$

and by the gravitational velocity:

$$V_g = \left(\frac{2g}{9\nu}\left(\frac{\rho_{p,i}}{\rho_{air}}\right) r_p^2\right) C_c \tag{4.42}$$

where k is the Bolzmann constant, T the ambient temperature, ν the air kinematic velocity, ρ_{air} the air density, g the gravitational acceleration, $\rho_{p,i}$ the aerosol density of mode i, and $C_c = 1 + 1.246\frac{\lambda_{air}}{r_p}$ the gliding coefficient. These expressions need to be averaged on the k^{th} moment and mode i as:

$$\hat{X} = \frac{1}{M_{k,i}} \int_{-\infty}^{\infty} X r_p^k n_i (\ln r_p) d(\ln r_p) \tag{4.43}$$

where X represents either D_p or v_g. After integration, we obtain for Brownian diffusivity:

$$\hat{D}_{p_{k,i}} = \tilde{D}_{p_{g,i}} \left[\exp\left(\frac{-2k+1}{2}\ln^2\sigma_{g,i}\right) + 1.246 K n_g \exp\left(\frac{-4k+4}{2}\ln^2\sigma_{g,i}\right)\right] \tag{4.44}$$

with $\tilde{D}_{p_{g,i}} = \left(\frac{kT}{6\pi\nu\rho_{air}R_{g,i}}\right)$
and for gravitational velocity:

$$\hat{Vg}_{p_{k,i}} = \tilde{Vg}_{p_{g,i}} \left[\exp\left(\frac{4k+4}{2}\ln^2\sigma_{g,i}\right) + 1.246 K n_g \exp\left(\frac{2k+4}{2}\ln^2\sigma_{g,i}\right)\right] \tag{4.45}$$

with $\tilde{Vg}_{p_{g,i}} = \left(\frac{2g\rho_{p,i}}{9\nu\rho_{air}} R_{g,i}^2\right)$

Dry deposition

According to Seinfeld and Pandis (1997) and using the resistance concept of Wesely (1989), aerosol dry deposition velocity for the k^{th} moment and mode i is:

$$\hat{v}_{d_{k,i}} = (r_a + \hat{r}_{d_{k,i}} + r_a \hat{r}_{d_{k,i}} \hat{Vg}_{p_{k,i}})^{-1} + \hat{Vg}_{p_{k,i}} \tag{4.46}$$

where surface resistance $\hat{r}_{d_{k,i}}$ is given by

$$\hat{r}_{d_{k,i}} = \left[(\hat{Sc}_{k,i}^{-2/3} + 10^{-3/\hat{St}_{k,i}})\left(1 + 0.24\frac{w_*^2}{u_*^2}\right) u_*\right]^{-1} \tag{4.47}$$

Schmidt and Stokes number are respectively equal to $\hat{Sc}_{k,i} = \nu/\hat{D}_{p_{k,i}}$ and $\hat{St}_{k,i} = (u_*^2/g\nu)\hat{v}_{d_{k,i}}$. One can observe that the friction velocity u_* and the convective velocity w_* depend on meteorological and surface conditions.

Sedimentation

For sedimentation process, we can use the above parameterization of $\hat{Vg}_{p_{k,i}}$. When vertical resolution is high, it is necessary to use a classical time splitting to compute sedimentation fluxes. It can be noted that the sedimentation / deposition processing modifies the particle distribution with an important loss of large particles in comparison to the small ones. After integration of the three moments, the distribution does not preserve the log-normal shape. If we consider after sedimentation processing the distribution as log-normal, the reconstruction of log-normal parameters σ, R_g induces a decrease of σ and an increase of R_g. The variation of σ is stronger than the R_g one. Nevertheless, in nature sedimentation process must decrease simultaneously σ and R_g. Therefore, we cannot consider the integration of the three moments to solve this problem. Two choices are possible:

- Sedimentation process with σ fixed : $M_{6,i}$ can be computed by maintaining σ equal to the previous values:
$$M_{6,i} = M_{0,i}\left(\frac{M_{3,i}}{M_{0,i}}\right)^{1/3} \exp\left(-3/2\log(\sigma_g)^2\right)^6 \exp\left(18\log(\sigma_g)^2\right) \tag{4.48}$$
- Sedimentation process with R_g fixed : A simple combination of $M_{k,i}$ gives $M_{6,i}$ in function of $M_{0,i}$, $M_{3,i}$, and $R_{g,i}$ as:
$$M_{6,i} = \frac{M_{3,i}^4}{R_{g,i}^6 M_{0,i}^3} \tag{4.49}$$

To decrease σ and R_g, a solution is to consider alternatively both treatment of $M_{6,i}$ for each time step.

4.2.4 Scavenging and aqueous mass transfer

Washout and cloud aerosol collection are calculated in the MesoNH based upon first order principals. In- and below-cloud impaction scavenging by cloud droplets and raindrops uses a kinetic approach to calculate the aerosol mass transfer as:
$$\frac{dM_p}{dt} = -\Lambda_M M_p \tag{4.50}$$
where dMp/dt represents the aerosol dry mass transfer in the acquous phase, M_p the aerosol dry mass and Λ_M the path normalized scavenging coefficient (in s^{-1}). Upon Pruppacher and Klett (2000) the normalized scavenging coefficient for Brownian motion between dry aerosol and cloud droplets is determined by the semi-empirical formulation as:
$$\Lambda_M M_p = \frac{1.35 LWC D_p}{r_{cloud}^2} \tag{4.51}$$
where LWC is the Liquid Water Content in g cm^{-3}, D_p is the diffusivity of the particle in m^2 s^{-1} and r_{cloud} the cloud droplet radius in m. Whereas the normalized scavenging coefficient between dry aerosol and rain droplets can be calculated as Seinfeld and Pandis (1997):
$$\Lambda_M M_p = \frac{3}{2}\frac{E}{r_{rain}} F_{rain} \tag{4.52}$$
where E is the collection efficiency fully described in (Seinfeld and Pandis 1997; Tost et al. 2006), r_{rain} the radius of the rain droplets (in mm) and F_{rain} the effective precipitation flux in kg m^{-2} s^{-1}.
Within this scheme, efficiencies for three types of collections are calculated. Small particles are collected efficiently through Brownian diffusion, but the collection efficiency decreases with increasing particle size. Inertial impaction is important for large particles, with collection efficiencies approaching one for particles of diameter greater than 20 μm. Washout is the least efficient for particles with diameters ranging from

0.2 to 2.0 μm, where interception in difficult due to particles following the streamlines of air around the falling droplet. The in-cloud mass aerosol transfers into rain droplets by autoconversion and accretion processes have been introduced as described by Pinty and Jabouille (1998). The sedimentation of aerosol mass included in raindrops is solved using a time splitting technique with an upstream differencing scheme of the vertical flux as:

$$P_{asr} = \frac{m_{aero}}{m_{rain}\rho}\frac{d}{dz}(V_r\,\rho\,r_{rain}) \tag{4.53}$$

where P_{asr} is the raindrop aerosol mass sedimentation rate, m_{aero} the aerosol mass included in raindrops (in kg kg^{-1} of air), m_{rain} the rain water (in kg kg^{-1} of air), ρ the air density and V_r the raindrop sedimentation velocity (in m s^{-1}). The rerelease of aerosols into the air due to rain evaporation is assumed to be proportional to the water evaporated (Chin et al. 2000). However, this is likely to overestimate the release of aerosols due to evaporation as some evaporation of the rain results in smaller raindrops that still contain the aerosols.

4.3 References

Ackermann, I., H. Hass, M. Memmesheimer, A. Ebel, F. Binkowski, and U. Shankar, 1998: Modal aerosol dynamics model for Europe : development and first applications. *Atmos. Environ.*, **32**, 2981–2999.

Baldocchi, D. D., B. B. Hicks, and P. Camara, 1987: A canopy stomatal resistance model for gaseous deposition to vegetated surfaces. *Atmos. Environ.*, **21**, 91–101.

Binkowski, F. and S. Roselle, 2003: Models-3 community multiscale air quality (CMAQ) model aerosol component. 1. Model description. *J. Geophys. Res.*, **108(D6)**, 4183, doi:10.1029/2001JD001 409.

Binkowski, F. and Shankar, 1995: The regional particulate model 1. Model description and preliminary results. *J. Geophys. Res.*, **100(D12)**, 26 191–26 209.

Blanchard, D. C., 1983: The production, distribution, and bacterial enrichment of the sea-salt aerosol. *Air-Sea Exchange of Gases and Particles*, P. S. Liss and W. G. N. Slinn, Eds., D. Reidel, Norwell, Mass., 407–454.

Chin, M., R. Rood, S. J. Lin, J. F. Müller, and A. Thompson, 2000: Atmospheric sulfur cycle simulated in the global model GOCARD: Model description and global properties. *J. Geophys. Res.*, **105**, 24,671–24,687.

Evans, K., 1998: The spherical harmonic discrete ordinate method for three-dimensional atmospheric radiative transfer. *J. Atmos. Sci.*, **55**, 429–446.

Friedlander, S., 1977: *Smoke, dust, and haze, fundamentals of aerosols dynamics*. 2d ed., Oxford University Press.

Fuchs, N., 1964: *The mechanism of aerosols*. Pergamon Press Oxford.

Griffin, R., D. Dabdub, and J. Seinfeld, 2002: Secondary organic aerosol. 1. Atmospheric chemical mechanism for production of molecular constituents. *J. Geophys. Res.*, **107(D17)**, 4332, doi:10.1029/2001JD000 541.

Griffin, R., D. Dabdub, and J. Seinfeld, 2005: Development and initial evaluation of a dynamic species-resolved model for gas-phase chemistry and suze-resolved gas/particle partitioning associated with secondary organic aerosol formation. *J. Geophys. Res.*, **110**, D05 304, doi:10.1029/2004JD005 219.

Grini, A., P. Tulet, and L. Gomes, 2006: Dusty weather forecasts using the MesoNH mesoscale atmospheric model. *J. Geophys. Res.*, **111**, D19 205, doi:10.1029/2005JD007 007.

Jacob, D. J., 2000: Heterogenous chemistry and tropospheric ozone. *Atmos. Environ.*, **34**, 2131–2159.

Kondo, J. and H. Yamazawa, 1986: Measurement of snow surface emissivity. *Bound.-Layer. Meteor.*, **34**, 415–416.

Kulmala, M. A., A. Laaksonen, and L. Pirjola, 1998: Parametrization for sulfuric acid / water nucleation rates. *J. Geophys. Res.*, **103**, 8301–8307.

Lee, K., H. Chen, and J. Gieseke, 1984: Log-normally preserving size distribution for Brownian coagulation in the free-molecule regime. *Aerosol Sci. Technol.*, **3**.

Marticorena, B. and G. Bergametti, 1995: Modeling of the atmospheric dust cycle: 1. Design of a soil derived dust emission scheme. *J. Geophys. Res.*, **100**, 16,415–16,429.

Monahan, E. C., C. W. Fairall, K. L. Davidson, and P. J. Boyle, 1983: Observed inter-relations between 10 m winds, ocean whitecaps and marine aerosols. *Quart. J. Roy. Meteor. Soc.*, **109**, 379–392.

Myhre, G., A. Grini, J. Haywood, F. Stordal, B. Chatenet, D. Tanré, J. Sundet, and I. Isaksen, 2003: Modeling the radiative impact of mineral dust during the Saharan dust experiment (SHADE) campaign. *J. Geophys. Res.*, **108(D18)**, 8579, doi:10.1029/2002JD002 566.

Nenes, A., C. Pilinis, and S. Pandis, 1998: A new thermodynamic model for inorganic multicomponent atmospheric aerosols. *Aquatic Geochemistry*, **4**, 123–152.

Philips, W., 1975: Drag on small sphere moving throught a gas. *Phys. Fluids*, **18**, 1089–1093.

Pinty, J.-P. and P. Jabouille, 1998: A mixed-phase cloud parameterization for use in a mesoscale non-hydrostatic model: simulations of a squall line and of orographic precipitations. *Conf. on cloud physics, Everett, WA, Amer. Meteor. Soc.*, 217–220.

Pratsini, S., 1988: Simultaneous aerosol nucleation, condensation, and coagulation in aerosol reactors. *J. Colloid Interface Sci.*, **124**, 416–417.

Pruppacher, H. and J. Klett, 2000: *Microphysics of clouds and precipitation*. Kluwer academic publishers.

Pun, B., R. Griffin, C. Seigneur, and J. Seinfeld, 2002: Secondary organic aerosol. 2. Thermodynamic model for gas/partitioning of molecular constituents. *J. Geophys. Res.*, **107(D17)**, 4333, doi:10.1029/2001JD000 542.

Ravishankara, A., 1997: Heterogeneous and multiphase chemistry in the troposphere. *Science*, **276(5315)**, 1058–1065.

Saxena, P., A. Hudischewskyj, C. Seigneur, and J. Seinfeld, 1986: A comparative study of equilibrium approaches to the chemical characterization of secondary aerosols. *Atmos. Environ.*, **20**, 1471–1483.

Schulz, M., G. de Leeuw, and Y. Balkanski, 2004: Sea-salt aerosol source functions and emissions. *Emissions of atmospheric trace compounds*, P. A. C. Granier and C. E. Reeves, Eds., Kluwer, 333–359.

Seinfeld, J. and S. Pandis, 1997: *Atmospheric Chemistry and Physics*. Wiley interscience pub.

Tost, H., P. Jockel, A. Kerkweg, R. Sander, and J. Lelieveld, 2006: Technical note: A new comprehensive scavenging submodel for global atmospheric chemistry modelling. *Atmos. Chem. Phys.*, **6**, 565–574.

Tulet, P., V. Crassier, F. Cousin, K. Suhre, and R. Rosset, 2005: ORILAM, a three moment lognormal aerosol scheme for mesoscale atmospheric model. on-line coupling into the Meso-NH-C model and validation on the Escompte campaign. *J. Geophys. Res.*, **110**, D18 201, doi:10.1029/2004JD005 716.

Tulet, P., M. Mallet, V. Pont, J. Pelon, and A. Boone, 2008: The 7-13 March 2006 dust storm over West Africa: Generation, transport, and vertical stratification. *J. Geophys. Res.*, **113**, D00C08, doi:10.1029/2008JD009 871.

van Pul, W. A. J. and A. F. G. Jacobs, 1994: The conductance of a maize crop and the underlying soil to ozone under various environmental conditions. *Bound.-Layer. Meteor.*, **69**, 83–99.

Vignati, E., G. DeLeeuw, and R. Berkowicz, 2001: Modeling coastal aerosol transport and effects of surf-produced aerosols on processes in the marine atmospheric boundary layer. *J. Geophys. Res.*, **106(D17)**, 20,225–20,238.

Walmsley, W. and M. L. Wesely, 1996: Modification of coded parameterizations of surface resistances to gaseous dry deposition. *Atmos. Environ.*, **30**, 1181–1188.

Wesely, M. L., 1989: Parameterization of surface resistances to gaseous dry deposition in regional-scale numerical models. *Atmos. Environ.*, **23**, 1293–1304.

Whitby, E., P. McMurry, U. Shankar, and F. Binkowski, 1991: Modal aerosol dynamics modeling. *Atm. Res. and Exposure Asses. Lab., U.S. Environ. Prot. Agency*.

Wilemski, G., 1984: Composition of the critical nucleus in multicomponent vapor nucleation. *J. Chem. Phys.*, **80**, 1370–1372.

Zender, C., H. Bian, and D. Newman, 2003: The mineral dust entrainment and deposition (DEAD) model: Description and global dust distribution. *J. Geophys. Res.*, **108(D14)**, 4416, URL http://dust.ess.uci.edu/dead/.

Zender, C., R. Miller, and I. Tegen, 2004: Quantifying mineral dust mass budgets: Terminology, constraints, and current estimate. *Eos Trans*, **85**, 509–512.

Chapter 5

Clouds Processing of Aerosols

Contents

Not yet implemented

5.1 References